Review

Current Status and Prospects on High-Precision Quantum Tests of the Weak Equivalence Principle with Cold Atom Interferometry

Liang Yuan, Jizhou Wu and Sheng-Jun Yang

Current Status and Prospects on High-Precision Quantum Tests of the Weak Equivalence Principle with Cold Atom Interferometry

Liang Yuan [1] , Jizhou Wu [2] and Sheng-Jun Yang [1,3,4,*]

1 Shenzhen Institute for Quantum Science and Engineering, School of Science, Southern University of Science and Technology, Shenzhen 518055, China; 12131223@mail.sustech.edu.cn
2 Department of Physics, Southern University of Science and Technology, Shenzhen 518055, China; wujz3@sustech.edu.cn
3 International Quantum Academy, Shenzhen 518048, China
4 Guangdong Provincial Key Laboratory of Quantum Science and Engineering, Southern University of Science and Technology, Shenzhen 518055, China
* Correspondence: yangsj@sustech.edu.cn

Abstract: For a hundred years, general relativity has been the best theory to describe gravity and space–time and has successfully explained many physical phenomena. At the same time, quantum mechanics provides the most accurate description of the microscopic world, and quantum science technology has evoked a wide range of developments today. Merging these two very successful theories to form a grand unified theory is one of the most elusive challenges in physics. All the candidate theories that wish to unify gravity and quantum mechanics predict the breaking of the weak equivalence principle, which lies at the heart of general relativity. It is therefore imperative to experimentally verify the equivalence principle in the presence of significant quantum effects of matter. Cold atoms provide well-defined properties and potentially nonlocal correlations as the test masses and will also improve the limits reached by classical tests with macroscopic bodies. The results of rigorous tests using cold atoms may tell us whether and how the equivalence principle can be reformulated into a quantum version. In this paper, we review the principles and developments of the test of the equivalence principle with cold atoms. The status of the experiments and the key techniques involved are discussed in detail. Finally, we give an outlook on new questions and opportunities for further exploration of this topic.

1. Introduction

Since Newton's theory of gravity was published more than 300 years ago, and Einstein's general relativity (GR) was further developed about 100 years ago, astonishingly good predictions and observations of the position and motion of matter have been achieved, from planets in the vast universe to objects in our everyday lives. Gravity is usually treated as a universally coupled force for all matter regardless of its properties and structure and can be considered as a geometric description of space–time in general relativity. However, it is widely accepted that the universe is expanding based on astronomical observations [1]. Currently, only 4.9% of the matter in the universe has been detected, and the existence of dark matter and dark energy has been postulated [2]. Quantum mechanics, on the other hand, governs physics at the microscopic scale, where matter has no definite trajectory and is described by wave functions. For now, properties of nonlocal entanglement and coherent correlations between microscopic particles have been rigorously demonstrated in all kinds of experiments [3–7]. The quantum field theory, particularly the Standard Model (SM),

provides a unified description of the electromagnetic, weak, and strong interactions except gravity [8]. Despite the persistent efforts since Einstein, the unification of gravity and quantum theories remains an unresolved issue in physics. Whatever is for sure, testing gravity in the framework of quantum mechanics should lead us to a whole new understanding of the world.

The universal coupling property of gravity, known as the Einstein equivalence principle (EEP) [9], is the cornerstone of the GR [10] and other gravitational geometry theories [11]. The EEP contains three different ingredients: the weak equivalence principle (WEP), the local position invariance (LPI) and the local Lorentz invariance (LLI). The last two ingredients describe the invariance in a local non-gravitational experiment: for any local non-gravitational experiment, the experimental results are independent of the velocity and location in the spacetime of the laboratory [12] As the foundation and a key ingredient of EEP, the WEP, asserts the equivalence between the gravitational and inertial masses of a particle, and it states that all point-like neutral particles experience the same free-fall trajectories, i.e., the same gravitational accelerations, independent of the composition, mass and material of these particles [13]. Thus, the WEP is also called the universality of free fall (UFF).

Tests of the WEP hypothesis are crucial for validating Einstein's theory or other candidate theories beyond Einstein's theory. In fact, all the new candidate theories beyond the GR and SM, including string theory [14,15], loop quantum gravity theory [16], Standard-Model Extension [17], dilaton model [18] and the fifth force [19,20], require the WEP to be broken. Also, some novel physical phenomena, such as new interactions [21], dark matter [22] and dark energy [23], that relate to gravity can also be found/checked by verifying the WEP.

In order to verify the correctness of the above candidate theories and promote the birth of a unified theory, the traditional test of the WEP has been developed in different macroscopic domains since Galileo's Leaning Tower experiments [24], such as the earliest single pendulum experiments (with an uncertainty of 10^{-6}) [25], mass drops (uncertainty of 10^{-10}) [26,27], torsion balances (uncertainty of 10^{-13}) [28,29] and Lunar Laser Ranging (uncertainty of 10^{-14}) [30,31], to name a few. Recently, MICROSCOPE reported the highest accuracy of the WEP test at about 1.5×10^{-15} by comparing the free-fall accelerations of two masses of titanium and platinum aboard a satellite in space [32,33].

All the results strongly confirm the equivalence between inertial and gravitational masses and the great success of the GR theory, and no evidence of WEP breaking was observed. However, we are still unclear whether the WEP still holds with higher accuracy and quantum effects taken into consideration. Theoretical studies suggest that the WEP test with atoms has a potentially higher accuracy than the WEP test with macroscopic objects [34,35]. It should be of interest to test the range of applications of the WEP with microscopic particles where quantum phenomenon become significant and will help us to understand the interplay between gravity and quantum physics. Due to the abundant degrees of freedom among the microscopic particles, it is also worth performing WEP verification experiments utilizing atoms with different properties, such as the proton and neutron number, the internal quantum states or spin and the nonlocal correlations that may lead to the coupling interaction between gravity and other forces. Meanwhile, some theories suggest that microscopic particles will exhibit different behaviors compared to macroscopic objects that would violate the WEP. For example, macroscopic objects are insensitive to the chameleon field due to the shielding mechanism; nevertheless, the atoms in vacuum can interact with the field [36–40]. Similar examples showing such distinction between atoms and macroscopic objects could be the case when the atoms have the controllable spin degree of freedom, and the spin-torsion coupling in gravity field, which is absent in the macroscopic objects, would break the WEP [41–46]. These studies will provide directions or clues to explore new mechanisms and interactions that may lead to the WEP breaking.

Here we focus on the topic of the quantum test of the WEP with cold atom ensemble. Due to the development of quantum information science and cold atom physics in

the last three decades, atom interferometers have been developed maturely for measuring gravity acceleration and gravity gradients [47,48]. It has shown great promise for applications in geophysics and mapping [49–51], civil engineering [52,53] and metrological standards [54–56]. In addition, it is also critically important for the exploration of fundamental physics, such as measurement of the gravitational constant G [57,58] and the fine-structure constant α [59–61], the test of the equivalence principle [62–64] and the detection of the gravitational waves [65–67]. Because of the potential applications of the cold-atom interferometers as inertial sensors with high accuracy in gravity measurements, and the well-defined and controllable properties of atoms, lots of quantum tests of the WEP with cold atoms have been proposed and carried out in the last two decades. In this review, we first provide a brief theoretical description of the WEP test using a cold atom interferometer in Section 2. A comprehensive overview about experiments of the WEP test using cold atoms is presented in Section 3, and the key techniques and systematic effects involved are summarized in Section 4. Finally, we offer some discussions on the prospects and opportunities for further exploration of this topic.

2. Basic Theory

In this section, we briefly introduce how atom interferometry works in the WEP test, which should suffice for discussions of the experimental and technical issues of the WEP test in the following sections. More introductions and reviews of the theoretical treatments of the WEP test can be found in [18,63].

As mentioned in the introduction, the WEP means the equivalence of the gravitational and inertial masses, which is expressed as $m_g = m_i$ with m_g and m_i being the gravitational mass and inertial mass, respectively. The breaking of the WEP is manifested as the breaking of the equality. After including the possible breaking terms, the relationship between these two masses can be written as [68]

$$m_g = m_i + \sum_{\mathcal{H}} \eta^{\mathcal{H}} \frac{E^{\mathcal{H}}}{c^2} = m_i \left(1 + \sum_{\mathcal{H}} \eta^{\mathcal{H}} \frac{E^{\mathcal{H}}}{m_i c^2} \right), \tag{1}$$

where $E^{\mathcal{H}}$ is the internal energy of the a known or unknown interaction $\mathcal{H}$ that may contribute differently to the gravitational and inertial masses, and c is the speed of light. $\eta^{\mathcal{H}}$ is a dimensionless parameter quantifying the violation of the WEP. If $\eta^{\mathcal{H}} \neq 0$, the WEP breaks.

To measure the violation parameters, we consider two bodies A and B with different masses dropping in a gravitational field. With the considered interactions from $\{\mathcal{H}\}$, their accelerations can be described by

$$a_{\{A,B\}} = \left(1 + \sum_{\mathcal{H}} \eta^{\mathcal{H}} \frac{E^{\mathcal{H}}_{\{A,B\}}}{m_{i,\{A,B\}} c^2} \right) g \tag{2}$$

with g being the acceleration of gravity. The acceleration difference of the two objects in the same gravitational field can be expressed by the Eötvös ratio as [68]

$$\eta \equiv 2 \left| \frac{a_A - a_B}{a_A + a_B} \right| \simeq \sum_{\mathcal{H}} \eta^{\mathcal{H}} \left| \frac{E^{\mathcal{H}}_A}{m_{iA} c^2} - \frac{E^{\mathcal{H}}_B}{m_{iB} c^2} \right|. \tag{3}$$

The zeros of all $\eta^{\mathcal{H}}$s, which lead to $\eta = 0$, signify the validation of the WEP. Practically, because the measurable η provides an upper bound of $\eta^{\mathcal{H}}$ [69], we use η as an indicator to test the WEP. Thus, the experimental test of the WEP goes to check the relative acceleration difference between the bodies A and B.

When we go to the quantum regime for the WEP test, we can use atoms with different properties as the two bodies A and B, and measure their acceleration in the gravitational field using an atom interferometer. We can use optical interferometers to analogize and

understand atom interferometers, where atoms instead of photons fly along different paths and interfere. Given atoms with a Λ-type energy structure of the states $|1\rangle$, $|2\rangle$ and $|i\rangle$ with "$|i\rangle$" denoting the intermediate (or excited) state, the Raman light consists of two laser beams which propagate in the opposite directions parallel to gravity and satisfy the two-photon resonance condition with the states $|1\rangle$ and $|2\rangle$. We use these two laser beams to split, reflect and recombine the wave packet of the atoms as shown in Figure 1. Usually, the laser frequencies are sufficiently far detuned from the transition frequency from the excited states to the state $|1\rangle$ or $|2\rangle$. Thus, the spontaneous emission can be neglected.
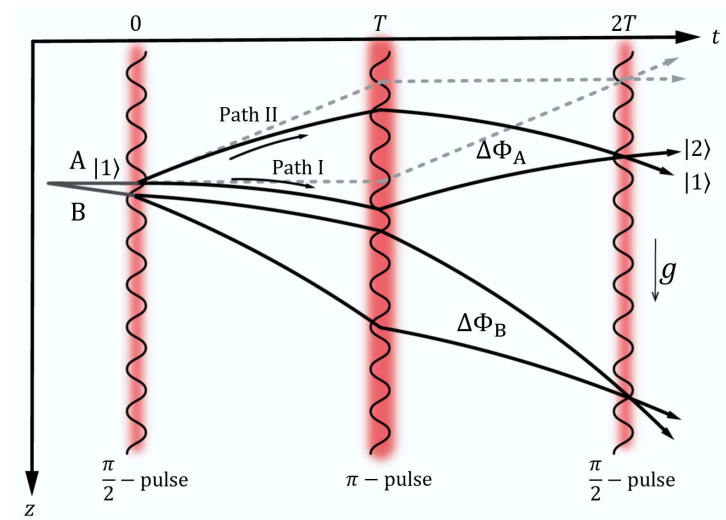

Figure 1. Schematic of the March–Zehnder atom interferometer using the $\frac{\pi}{2}$-π-$\frac{\pi}{2}$ Raman pulses. T represents the free evolution time between the Raman pulses. The three Raman pulses are used for splitting, reflection and recombination of the atomic wave packets. Path I and II mean the two arms of the interferometer. The gray line in the figure represents the classical interference path of the matter wave in the absence of gravity, and the black line represents the path in the presence of gravity. A and B label atoms of different natures for the test of the WEP. $\Delta\Phi_A$ and $\Delta\Phi_B$ are the phase change produced by gravity acceleration g, and the Eötvös parameter η can be obtained from the comparison between them.

Initially, the atoms are prepared in the state $|1\rangle$. At $t = 0$, half of the atoms are transferred to the state $|2\rangle$ by a $\frac{\pi}{2}$-Raman pulse, and the remaining half are still in $|1\rangle$. Then, the atoms fall freely in the gravity field and separate in the free space into Path I for the atoms remain in $|1\rangle$ and Path II for the transferred atoms in $|2\rangle$ due to an extra momentum $\hbar k$ from photons, respectively. Here, k is the wave number of the Raman light. At $t = T$, one π-pulse acts on the atoms to flip the atomic states. Atoms in Path I gain a momentum of $\hbar k$ and flip to the state $|2\rangle$, and atoms in Path II gain a momentum of $-\hbar k$ and flip to $|1\rangle$. After another flying time T, atoms in the two paths will recombine. At this time, another $\frac{\pi}{2}$-Raman pulse is applied to merge the wave packets and interfere. Any physical effect induces a different phase for the different paths, leading to an interference pattern in the atomic distribution.

For each atom ensemble A or B, the final population of atoms on the ground state $|1\rangle$ can be expressed as

$$P = P_{\text{off}} + P_{\text{amp}} \cos(\Delta\Phi), \tag{4}$$

where P_{off} and P_{amp} are the offset and amplitude of the interference fringe, respectively, and $\Delta\Phi$ is the phase difference between paths I and II written as [70]

$$\Delta\Phi = kaT^2 - 2\pi\alpha T^2 \tag{5}$$

with α being the chirp rate of the two-photon frequency of the Raman pulse to compensate for the Doppler shift and a being our target, which is used to determine the Eötvös ratio

η as per Equation (3). Thus, by measuring $\Delta\Phi$ accurately, we can get the value of the acceleration a using Equation (5). Alternatively, the Eötvös ratio can be determined from the differential of the phases between two ensembles of atoms in the atom interferometers. The measurement sensitivity depends on the transfer momentum k and the flying time T, which determine the enclosed area of the atom interference. There are other atom interferometry schemes using various wave packet split and recombination methods, like Bragg diffraction [71–73], Bloch oscillation [74–77] and composite pulses [78–81] to measure a. We briefly discuss these methods later in Section 4.

With a_A and a_B retrieved from the measured $\Delta\Phi_A$ and $\Delta\Phi_B$, the Eötvös ratio between atoms A and B can be calculated using Equation (3). The detection accuracy of η depends on the performance of the atom interferometers, including the precision, sensitivity and stability. There are many different factors that can contribute as the noise in the experiments. One example is that if trajectories of atoms A and B do not coincide as shown in Figure 1, the introduced systematic error can make us misinterpret the measured value of η. Keeping the test atoms in the same region with the same trajectories can suppress the common-mode noise [82], which needs very delicate efforts. To reach high accuracy of the WEP test, other key factors are discussed in Section 4.

In addition, besides the two atom ensembles A and B being independent of each other, coherent superposition and nonlocal correlation between them can be prepared. These quantum effects may contribute to the modifications of the inertial and gravitational masses [83–86]. In addition, when we use quantum to describe the gravitational fields, entangled particles can be used to test quantum form WEP [87]. Thus, the cold atom interferometer also provides us opportunities to check quantum aspects of the WEP.

3. Developments and State of the Art

Shortly after the successful laser cooling and trapping of atoms [88–90], the first demonstration of gravity measurement using cold atom interferometry was published in 1991 [91]. In 1999, the same group measured gravity with an uncertainty of $\Delta g/g \sim 3 \times 10^{-9}$. Though they did not intend to test the WEP, they compared gravity measured using their atom interferometer with that measured using a Michelson gravimeter, which is a free-fall type absolute gravimeter with a macroscopic glass corner cube. The relative difference between these two measured gravity values is within 7×10^{-9} [92]. The techniques of using a macroscopic classical object and a microscopic quantum object to test the WEP were developed maturely in 2021 [56]. Due to the advantages of the controllable, well-defined and high repeatability of cold atoms, the WEP test using two ensembles of atoms, which has a higher prospects for ultimate sensitivity, is more attractive compared to the WEP test using both atoms and macroscopic objects [93]. There are also other proposals for the WEP tests with other microscopic particles, such as using neutral antimatter [94,95], molecules with different conformations and chiralities [96]. Most of the current efforts are focused on reducing the temperature of these particles and perform efficient matter-wave interference [97–99]. The research is still in the primary stage. In this review, we only focus on the cases when bodies A and B both are atoms.

The first WEP test using the two bodies of atoms was performed with the two rubidium isotopes of ^{85}Rb and ^{87}Rb with a relative accuracy of $\sim 10^{-7}$ in 2004 [100]. The main technique they used in their atom interference is the Bragg diffraction, which is also applied in gravity measurement with a sensitivity of $6 \times 10^{-8}\,\mathrm{g}/\sqrt{\mathrm{Hz}}$ [101]. Compared to the Bragg-diffraction atom interferometers, the Raman-pulse atom interferometer introduced in Section 2 is more prevailing in the WEP test due to its simplicity and feasibility with looser requirements on the lasers. The Raman-pulse atom interferometer has been developed for gravity measurement since 1991 [91], such as reducing the systematic errors [70,92,102], increasing the fall-down time [103–105] and reducing the size of the interferometer for commercial or practical applications [106–111]. Currently, the Raman-pulse gravity measurement has reached the resolution of $4.5 \times 10^{-11}\,\mathrm{g}/\mathrm{shot}$ reported by the Zhan group [105] and the potential acceleration sensitivity of $6.7 \times 10^{-12}\,\mathrm{g}/\mathrm{shot}$ given

by the Kasevich group [104]. The above development of gravity measurement with atom interferometers has laid a good foundation for the WEP test.

Here, we review the main experiments of the WEP tests using cold-atom interferometers up to now and sort them out into three categories as shown in Table 1 and Figure 2, which are the WEP tests using dual atomic species reviewed in Section 3.1, dual atomic isotopes reviewed in Section 3.2 and dual atomic internal states reviewed in Section 3.3.

Table 1. Summary of the main experimental results of the WEP test with cold atoms performed in the past two decades.

| Properties of the Test Bodies		Year	Accuracy (η)	Group & Reference
Dual-species	$^{87}Rb - ^{39}K$	2014	$(0.3 \pm 5.4) \times 10^{-7}$	LUH [112]
	$^{87}Rb - ^{39}K$	2015	$(- - \pm 1.6) \times 10^{-6}$ per shot	LP2N [113]
	$^{87}Rb - ^{39}K$	2016	$(0.9 \pm 3.0) \times 10^{-4}$ @ $0g$	LP2N [114]
	$^{87}Rb - ^{39}K$	2020	$(1.9 \pm 3.2) \times 10^{-7}$	LUH [115]
	$^{87}Rb - ^{39}K$	2022	$(0.9 \pm 1.6) \times 10^{-6}$	LP2N [116]
Dual-isotopes	$^{85}Rb - ^{87}Rb$	2004	$(1.2 \pm 1.7) \times 10^{-7}$	MPIQ [100]
	$^{85}Rb - ^{87}Rb$	2013	$(1.2 \pm 3.2) \times 10^{-7}$	ONERA [117]
	$^{88}Sr - ^{87}Sr$	2014	$(0.2 \pm 1.6) \times 10^{-7}$	LENS [118]
	$^{85}Rb - ^{87}Rb$	2015	$(2.8 \pm 3.0) \times 10^{-8}$	WIPM [82]
	$^{85}Rb - ^{87}Rb$	2018	$(6 \pm - -) \times 10^{-11}$ per shot	Stanford [119]
	$^{85}Rb - ^{87}Rb$	2020	$(1.6 \pm 3.8) \times 10^{-12}$	Stanford [120]
	$^{85}Rb - ^{87}Rb$	2021	$(0.8 \pm 1.4) \times 10^{-10}$	WIPM [121]
Dual-states	$^{85}Rb, |2\rangle - |3\rangle$	2004	$(0.4 \pm 1.2) \times 10^{-7}$	MPIQ [100]
	$^{87}Rb, m_F = \pm 1$	2016	$(0.2 \pm 1.2) \times 10^{-7}$	HUST [122]
	$^{87}Rb, |1\rangle - |2\rangle$	2017	$(1.0 \pm 1.4) \times 10^{-9}$	LENS [123]
	$^{87}Rb, |1\rangle - |2\rangle$	2020	$(0.9 \pm 2.7) \times 10^{-10}$	HUST [124]
	$^{87}Rb, |1\rangle - |2\rangle$	2022	$(0.9 \pm 2.9) \times 10^{-11}$	HUST [125]
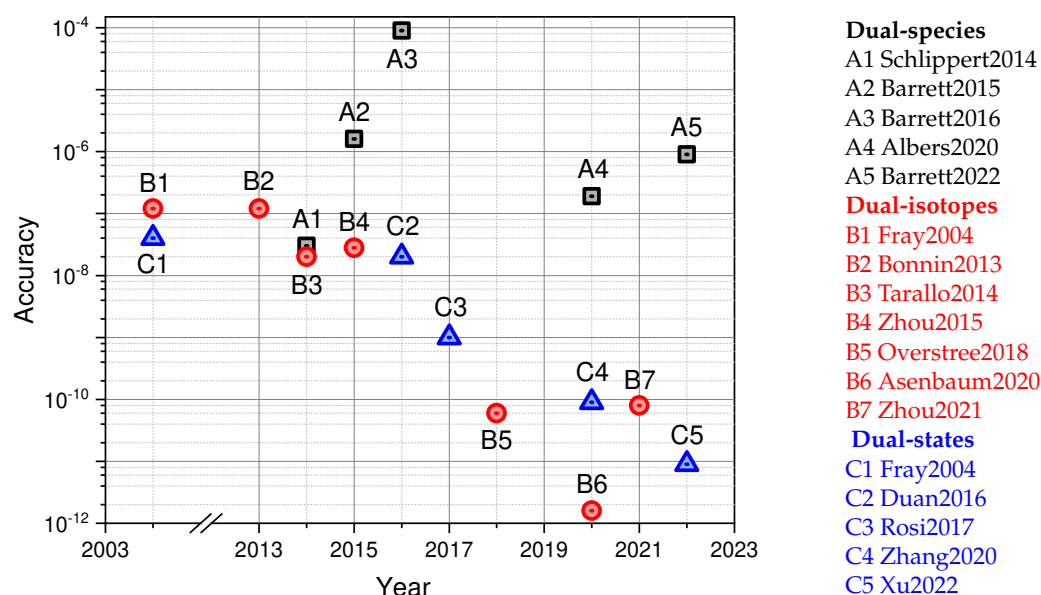
Figure 2. Measurement accuracy of the the Eötvös parameters η in the WEP tests with cold atoms. The black, red and blue points represent results using dual-species (A1 [112], A2 [113], A3 [114], A4 [115], A5 [116]), dual-isotopes (B1 [100], B2 [117], B3 [118], B4 [82], B5 [119], B6 [120], B7 [121]), and dual-states (C1 [100], C2 [122], C3 [123], C4 [124], C5 [125]) atom interferometers respectively, as listed in Table 1.

3.1. Dual Atomic Species

First, we discuss the WEP tests using a dual-species atom interferometer. Compared with the isotopes case, cooling and trapping two atomic species at the same time need more lasers and other equipment. The two species of atoms are controlled by lasers with significantly different wavelengths, which leads to asynchronous interference paths of the atoms. As a result, though large differences in mass and composition will make them more sensitive to possible WEP breaking effects [126], the experimental test with different atomic species is challenging due to the complex apparatus and systematic error correction. Until now, most two-species experiments have been conducted using ^{87}Rb and ^{39}K atoms, but the precision achieved is relatively low [112–116].

In 2014, Schlippert et al. conducted the WEP test in two Raman-type atom interferometers with laser-cooled ensembles of ^{87}Rb and ^{39}K [112]. They eliminated the noninertial phase shifts by alternately recoiling the atoms in the opposite directions and taking half difference between them. They obtained the Eötvös parameter $\eta = (0.3 \pm 5.4) \times 10^{-7}$ [112], of which the standard uncertainty was improved to 3.2×10^{-7}, by increasing the free-falling time in 2020 [115]. Their accuracy was mainly limited by the second-order Zeeman effect and the wavefront curvature of the Raman beams. In 2015, the LP2N group proposed a dual-species fringe reconstruction by accelerometer correlation method to realize a common mode suppression ratio of 730 for the vibration noise and obtained an Eötvös parameter of 1.6×10^{-6} per measurement at a free evolution time of 10 ms [113]. The next year, they tested the WEP in a weightless environment produced during a parabolic flight [114]. The Eötvös parameter was measured with the uncertainty of 3.0×10^{-4} in the microgravity, which is four times better than that in the standard gravity. In 2022, they improved the interrogation time to $T = 20$ ms and obtained the accuracy of $\eta = (0.9 \pm 1.6) \times 10^{-6}$ [116]. The statistical uncertainty of the Eötvös parameter is 7.8×10^{-8} after 2.4×10^4 s of integration. Tests with other atoms, such as ^{87}Rb and ^{170}Yb [127], and Cd and Sr [128], are still in progress.

3.2. Dual Atomic Isotopes

Since isotopes of the same atomic species have similar transition frequencies; the corresponding WEP tests are much less complex compared to the above experiments with different atomic species. Nearly one decade after the first WEP test [100], the ONERA group reported a matter-wave interferometer that simultaneously interrogates isotopes of ^{85}Rb and ^{87}Rb. Their measured relative differential acceleration $\Delta g/g$ is $(1.2 \pm 3.2) \times 10^{-7}$ with a resolution of 2.5×10^{-8} [117]. In 2014, the Tino group reported a new test of the WEP using two isotopes of strontium atoms, namely, the bosonic ^{88}Sr and the fermionic ^{87}Sr [118]. By measuring the Bloch frequencies of ^{88}Sr and ^{87}Sr, they obtained $\eta = (0.2 \pm 1.6) \times 10^{-7}$. The main error sources come from the frequency shift of the Raman light and the Coriolis force. In 2015, the Zhan group proposed and implemented a four-wave double-diffraction Raman transition (FWDR) scheme to suppress the common-mode phase noises of the Raman lasers in the ^{85}Rb-^{87}Rb dual-species atom interferometer [82]. The accuracy of the measured η is $(2.8 \pm 3.0) \times 10^{-8}$, and the statistical uncertainty is 0.8×10^{-8} after 3200 s of integration. In 2021, the same group improved the accuracy of the WEP test to $(0.8 \pm 1.4) \times 10^{-10}$ [121]. In 2018, the Kasevich group suppressed gravity-gradient-induced phase differences by selecting the appropriate Raman pulse frequency shift with a relative precision of $\Delta g/g$ being about 6×10^{-11} per shot [119]. In 2020, they demonstrated zero violation of the WEP between ^{85}Rb and ^{87}Rb with the accuracy at the level of 10^{-12} [120], which is the highest accuracy so far by using microscopic particles. Further, proposals and ongoing experiments with dual-isotopes aim to achieve a precision of 10^{-15} or better [129,130].

3.3. Dual Atomic Internal States

In addition to the above tests for atoms that have different masses, a new class of experiments has been proposed to use different energy states of the same atoms. According to Einstein's mass–energy equation, atoms at different energy states are different in their

equivalent mass. Their different internal states also bring us opportunities to check the potential quantum effects in gravity and the coupling interactions between gravity and the other forces.

In 2004, Fary et al. performed the early WEP test using the ^{85}Rb atoms in the hyperfine ground states $F = 2$ and $F = 3$ and obtained gravity acceleration difference within $(0.4 \pm 1.2) \times 10^{-7}$ [100]. Using the same atoms but with opposite-spin-oriented states, i.e., ^{85}Rb atoms with $m_F = 1$ and $m_F = -1$, a group from HUST carried out a test of the WEP with the measured Eötvös parameter being $(0.2 \pm 1.2) \times 10^{-7}$ [122]. In 2020, their result is improved to $\eta = (0.9 \pm 2.7) \times 10^{-10}$ by using the Bragg-diffraction atom interferometer with the hyperfine ground states $|F = 1, m_F = 0\rangle$ and $|F = 2, m_F = 0\rangle$ of ^{87}Rb atoms [124]. Recently, they further improved the upper bound of the WEP test to 2.9×10^{-11} [125]. In 2017, the Tino group also realized quantum test of the WEP for the ^{87}Rb atoms in coherent superposition of internal states $|F = 1, m_F = 0\rangle$ and $|2, 0\rangle$ [123]. They used Bragg atom interferometers in a gravity gradiometer configuration and achieved a relative uncertainty of the Eötvös parameter at the low level of 10^{-9}.

Incorporated with atoms of different masses and different internal states simultaneously, the joint mass–energy test of the WEP using the isotopes of ^{85}Rb and ^{87}Rb was carried out by Zhou et al. in 2021, and the accuracy of the η is at the level of 10^{-10} [121]. The chance of the WEP violation increases with the increased energy difference between the internal states. Thus, a larger energy separation is expected in the future [18]. In addition, tests of the equivalence principle with squeezing, entanglement and nonlocal correlation of the atomic states are also significant.

4. Key Techniques and Systematic Effects

Current accuracy of the Eötvös parameter η is at the level of 10^{-11} for different internal states of the same species and 10^{-12} for different isotopes but only 10^{-7} for different atom species. This is far away from the accuracy of 10^{-15} using the macroscopic classical masses [32]. Thus, to achieve the high precision in the WEP test with atom interferometers, one main challenge that we should put in the first priority is to obtain higher sensitivity, accuracy and stability of gravity measurement. Currently, the sensitivity of gravity measurement using atom interferometers is at the level of $10^{-9}\, \mathrm{g}/\sqrt{\mathrm{Hz}}$, which is the key obstacle that limits accuracy improvements.

In addition, the atoms used for the WEP tests are mainly the alkali metals, especially the rubidium atoms. High-rate cooling and trapping of other atomic species is demanding for a richer variety of the WEP tests. Techniques for preparation of cold atomic sources will not be discussed in this review. Also, we do not explore all factors for carrying out the WEP tests but focus on some key techniques and systematic effects, such as preparation and control of laser pulse, atom trajectory and interference signal detection, gravity gradient, wavefront aberration and suppression of vibration noise and other major noises. Actually, what we focus on is the differential phase of the two components in the WEP test experiment with dual species. Through certain methods, most of the noise can be suppressed as common-mode noise, which we will discuss later in this section.

4.1. Preparation and Control of Laser Pulse

In a Raman-type atom interferometer, the Raman light is the core technology to split and reflect atoms, with which the hyperfine ground states of atoms are coupled through the two-photon resonance. In order to realize the two-photon resonance during the atom dropping, we need to tune the frequency of the Raman light to compensate the Doppler frequency drift. In the meanwhile, to realize stable and significant atom interference pattern, the active feedback technique is also necessary to eliminate the phase fluctuations and noises in the Raman pulses.

There are several methods to realize Raman light, including optical phase-locked loop (OPLL) [131,132], acousto-optic modulation (AOM) [133,134] and electro-optic modulation (EOM) [135,136]. The OPLL is used between two independent lasers, whose system

is complex and not conducive for miniaturization and integration. It has low noise in the low frequency range (10–100 Hz), but due to the influence of the feedback circuit, the phase noise in the high frequency range is extremely high [137]. The AOM scheme has significant low phase noise. However, the frequency shift of the AOM is generally lower than 5 GHz, and the diffraction efficiency is extremely low for the high frequency that requires large laser power. Wang et al. combined the OPLL and AOM schemes to achieve low phase noise with broad bands [138]. The general EOM scheme is compact and simple but will generate double sidebands, causing unwanted power waste and system errors [139,140].

Based on the electro-optic effect, a cascaded Mach–Zehnder interferometer is used to apply orthogonal phase modulation to the optical signal, which can achieve a method called optical single-sideband modulation. This technology tunes the ratio–frequency phase shifter and bias voltages on an in-phase/quadrature (I/Q) modulator and has achieved the reduction of errors caused by unnecessary sidebands [141,142]. The I/Q modulator is essentially a cascaded Mach–Zehnder interferometer, as shown in Figure 3. The main noise using single-sideband lasers comes from the fluctuations in the sideband/carrier ratio, which leads to the extra phase shift in gravity measurement [142]. In 2019, a portable atom gravimeter based on this simple optical protocol was implemented [143].
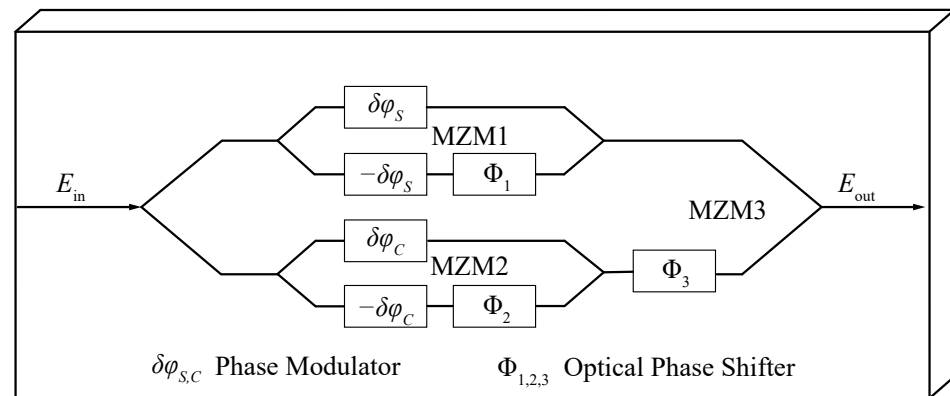

Figure 3. Internal diagram of an I/Q modulator. E_{in} and E_{out}: the input and output laser field; $\delta\phi_S = \beta\sin\omega_m t$ and $\delta\phi_C = \beta\cos\omega_m t$: the sine and cosine phase modulator; $\Phi_{1,2,3}$: optical phase shifter; MZM: Mach–Zehnder modulation.

As mentioned in Section 2, alternative methods. including Bragg diffraction [71–73] and Bloch oscillation [74–76], can also be used as beam splitters and mirrors to achieve the atom wave packet splitting and reflection. Different from the Raman pulse, the laser used in Bragg diffraction does not need high frequency modulation since it is a process of photon recoil momentum transfer in the same internal state. Thus, the Bragg method provides well rejection of the external field influence. Bloch oscillation, which forms a moving optical lattice by two counter-propagating laser beams with small frequency difference $\delta\nu$, can accelerate the atoms and achieve a large momentum transfer (LMT) beam splitter. Furthermore, we can improve sensitivity and accuracy of the atom interferometers by employing a sequence of light pulses, which combines the advantages of the techniques of Raman transition, Bragg diffraction and Bloch oscillation [144]. In addition to the ordinary two-photon or multi-photon transition schemes, there is also another scheme of atom interferometer based on the single-photon ultranarrow clock transition of strontium atoms, which greatly reduces susceptibility to the laser noise [145]. In addition, the cavity-enhanced light–atom interaction can provide advantage of power enhancement and spatial filtering and pave the way toward large-scale and high-sensitivity interferometer [146,147].

4.2. Atom Trajectory and Signal Detection

In the experiments, the phase that contains gravity information can be retrieved by detecting the population of atoms as per Equations (4) and (5). To minimize the errors in measuring the atoms' population, we need to trace the atom's trajectory and develop

techniques to analyze the detection signals. In this section, we introduce the developments of atom trajectory tracing technology and analysis methods for the signal detection.

There are two main concerns in atom trajectory. One is that the mismatch between the atom trajectory and Raman pulse sequence can lower the interference fringe contrast and increase the amplitude noise, which is the noise shown in P_{amp} in Equation (4). The effect of such mismatch is significant in experiments with large interference loop areas. The other one is the mismatch of atom trajectories of different components in the dual-species atom interferometer. When we extract the differential phase, the asynchronous drift of atoms of different species can reduce the level of common-mode noise suppression. Therefore, the symmetry and overlap of atom trajectories is crucial in the performance of dual-species atom interferometers. To trace the atom trajectory, Yao et al. proposed an experiment setup to include two sets of Raman lights in the atom interferometers, of which one set is along the moving direction of atoms to monitor the position of atoms, and the other set is vertical to the moving direction of atoms to measure the velocity of atoms [148]. In 2022, their setup was upgraded to introduce the active feedback control in the calibration of the atom trajectories, of which the stability was improved by two orders of magnitude [149].

In the detection, the experimental data are the fluorescence signals from the spontaneous radiation of the pumped-up atoms. The intensity of the signals gives us the atom population, which could be fluctuating due to the imbalance of intensities of the trapping lasers and the drift of the magnetic field. Such fluctuation in the total atom number, which is one cause of the amplitude noise, can be suppressed by a normalization detection method, such as the two-state sequential detection [150] and two-state simultaneous detection [151]. To further simplify the normalized detection process, Song et al. proposed to normalize the atomic population by the quenched fluorescence signals during initial state preparation [152].

In processing the data, different techniques have been developed to extract the differential phase signal $\Delta\Phi_A - \Delta\Phi_B$ in the dual-atom interferometer. In the case when the common-mode noise is comparable to the differential phase signal, where the least squares method may fail to fit the data, the method of ellipse fitting [153] can be used to extract the differential phase. However, the ellipse fitting method would introduce significant bias and may not provide the optimal fit with the prior knowledge of the noise. The problem was overcome by incorporating the ellipse fitting with the Bayesian estimation by Stockton et al. [154], which was applied to extract the differential acceleration with atoms of different masses in the proposal of Varoquaux et al. in 2009 [155]. Such a Bayesian estimation method was later developed by Chen et al. [156] and Barrett et al. [113]. Barrett et al. also applied a Bayesian estimation method in the WEP test experiments with K and Rb atoms [113]. In 2016, Wang et al. proposed to combine the linear and ellipse fitting methods to extract the differential phase [157]. This method can accurately extract the small differential phase in the noisy environment, which makes up for the shortcomings of the ellipse fitting method and the Bayesian statistics statistical method. There are also other techniques in data processing for some particular application scenarios, such as the spectrum correlation method for the WEP test using atoms in a spacecraft [158].

4.3. Major Systematic Effects

In this subsection, we introduce the main systematic effects that cause deviations in measurement results and review the methods of suppressing them.

4.3.1. Gravity Gradient and Coriolis Effect

The gravity gradient is one of the most serious systematic effects in the WEP test. Due to the Earth's gravitational field and mass distribution surrounding the atoms, The gravity acceleration is usually not constant along the trajectories of the atoms. gravity gradient can give rise to an additional phase shift as it couples to the initial velocity and position of the atoms [159]. For a cold atomic ensemble with an initial statistical distribution, there is an unavoidable phase uncertainty, especially for the long-baseline interferometer. In addition,

there exist higher-order systematic errors in the WEP test when different atoms move in different trajectories.

Roura proposed a scheme to overcome the influences of the gravity gradient and meet the requirements of the initial colocalization of two atom ensembles A and B by changing the effective momentum transfer in the Raman transition using the π-pulse at $t = T$ [160]. Shortly after, D'Amico et al. experimentally demonstrated this method and showed its promising high sensitivity and accuracy even in the presence of nonuniform forces [161]. Overstreet et al. created an effective inertial frame that could suppress the error of the gravity gradient to 10^{-13} g by selecting the appropriate frequency shift of Raman pulse [119]. In the spaceborne test of the WEP, Chiow et al. showed that the gravity inversion and modulation using a gimbal mount can suppress gravity gradient errors, which reduces the need to overlap two species of atoms [162].

Similar to the gravity gradient, the Coriolis effect, which is caused by the Earth's rotation, leads to one systematic error manifested as the deviation of the atoms' trajectories when the atoms initially possess the transverse velocity with respect to the incident laser beams [70]. Duan et al. presented detailed discussions on how to suppress the Coriolis error in the WEP test using a dual-species atom interferometer [163]. They reduced the uncertainty of the η introduced by the Coriolis force to 10^{-11} by rotating the Raman laser reflector. Lan et al. used a tip–tilt mirror to compensate the phase shift caused by the Coriolis force and improved the contrast of interference fringes [164]. Louchet-Chauvet et al. measured gravity values in the direction opposite to the Earth's rotation vector, separated the influence and corrected the Coriolis shift [165].

4.3.2. Wavefront Aberrations

Waveform aberrations, as one main factor that leads to the systematic uncertainty [166,167], are caused by the imperfections of the laser beam profiles and the retro-reflecting mirrors in the atom interferometers. Without any optimization, the uncertainty contribution of this factor in gravity measurement is on the level of 10^{-9} g, which strongly limits the accuracy of the WEP test. Wang et al. analyzed the influence of the wavefront curvature of Raman pulses by the method of a transmission matrix [168]. Schkolnik et al. presented a experimental analysis of wavefront curvature based on measured aberrations of optical windows. The uncertainty of the measured gravity is less than 3×10^{-10} g [166]. Zhou et al. presented a detailed theoretical analysis of wavefront aberrations and measured the effect by modulating the waist of Raman beams [169]. Trimeche et al. used deformable mirrors to actively control the laser wavefront and achieve compensation for wavefront curvature [170]. Hu et al. proposed an expansion-rate-selection method to suppress the aberration phase noise in the WEP test using dual-species atom interferometers [167]. The simulations showed that the suppressed uncertainty to the Eötvös parameter is on the level of 10^{-14} for isotopic atoms and 10^{-13} for nonisotopic atoms. Better results can be obtained by using atoms with lower temperature. Karcher et al. established a thorough model to study the influence of wavefront curvature on atom interferometer and proposed a method to correct for this bias based on the extrapolation of the measurements down to zero temperature [171].

4.3.3. Stark and Zeeman Effects

The Stark effect resulting from the laser beams is an important systematic error. Particularly for the WEP test with two atomic species, we need to use two lasers with different wavelengths, where the crosstalk between these two lasers may influence the results. One possible solution is to choose lasers with zero-magic or tune-out wavelengths to selectively manipulate the two atomic species [172].

The Zeeman effect caused by the inhomogeneous magnetic field can also lead to the error in the atom interferometer. For the magnetically insensitive states of atoms, i.e., the atomic states with $m_F = 0$, though the first-order term of the Zeeman effect is zero, the

nontrivial higher-order terms still exist due to the nonzero gradient of the magnetic field and contribute as one main error in the measurement of η when two bodies of atoms A and B experience the Zeeman effect differently. Such an error is especially significant for interference using two kinds of atoms. For example, the second-order term of the Zeeman effect in the K atom is 15 times that in the Rb atom.

An accurate evaluation of the second-order Zeeman effect can greatly improve the WEP verification accuracy. Hu et al. reported an experimental investigation of the Raman-spectroscopy-based magnetic field measurements. The second-order Zeeman effect in the atom interferometer is evaluated with this method, and the uncertainty is 2.04×10^{-9} g [173]. In addition to providing a stable magnetic field, establishing a magnetic shield in the region of the atom interference is also an irreplaceable method. Wodey et al. designed a modular and scalable magnetic shielding device for ultra long-baseline atom interferometer measurement systems, limiting the magnetic-field-related errors in atom interferometer to the 10^{-13} g level [174]. Ji et al. achieved a high-performance magnetic shielding system for a long-baseline atom interferometer by combining passive shielding of permalloy with active compensation of coils. The system is expected to reduce the error of quadratic Zeeman effect to the 10^{-13} level in the WEP test [175]. Hobson et al. solved the magnetic field distortion caused by magnetic shielding by designing multiple coils on the coil support to generate three uniform and three constant gradient fields [176].

4.3.4. Atoms Interaction and Self-Attraction Effect

To obtain high precise measurement of the gravity difference, atoms prepared in a Bose–Einstein condensate (BEC) would be an ideal candidate, but the phase shifts and errors introduced by the atomic interactions in BEC must be accurately calculated or estimated [177–180]. Jannin et al. proposed a theoretical model based on a perturbative approach for the precise calculation of the phase shift introduced by atom–atom interactions [177]. Yao et al. used the Feynman path integral method to evaluate the phase shift of atomic interactions, and the method is in good agreement with experimental results [179]. Burchianti et al. proposes that atom–atom interactions only introduce local phase shifts in the region where wave packets overlap [180].

The self-attraction effect caused by the gravitational force generated by the surrounding mass experimental devices is also one of the errors that needs to be evaluated [181,182]. Based on the finite element method, D'Agostino et al. presented a numerical method for the calculation of the self-gravity effect in atom interferometers [182]. The numerical uncertainty introduced by this effect is 10^{-9} g in the measurement of gravity.

4.4. Noise Suppression

Environmental vibration noise is one of the critical issues that needs to be overcome in the realization of high-precision atom interferometer. Ground and equipment vibrations, especially in the low frequency range between 0.01 Hz and 10 Hz, are transmitted to the reflector of the Raman beam, which influences the interference fringes. Thus, performing the WEP tests on the ground preferably requires a very quiet environment and passive and/or active vibration reduction.

Early in 1999, Steve Chu's group applied ultra-low-frequency active damping technology to reduce the vibration error of frequency from 0.1 Hz to 20 Hz by a factor of 300 [183]. The group from WIPM built the active vibration reduction system on one passive vibration reduction platform and suppressed the vertical vibration noise by 300 times from frequency of 0.1–10 Hz [184]. The HUST group developed a three-dimensional active vibration reduction system and solved the coupling problem between the horizontal and vertical vibrations [185]. This isolator is especially suitable for atom interferometers whose sensitivity is limited by the vibration noise. Common-mode vibration noise can be suppressed by 94 dB for a simultaneous dual-species atom interferometer [186]. Chen et al. proposed a proportional-scanning-phase method to reduce the vibration noise and pointed out that the

ratio of the induced phases by vibration noise is constant between two atom interferometers at every experimental data point [156].

As mentioned above, the noises of the Raman pulses (power, frequency, and phase), the asymmetric atom trajectories, the influence of gravity gradient, etc., can limit the precision of the measurement. One method is to eliminate them as common-mode noises for the two test bodies. Obviously, the atom interferometers using the same laser light on the two atom ensembles can reject most of the noises up to a large scaling factor. For atom interferometer experiments, Lévèque et al. adopted a double-diffraction Raman transition technique, as shown in Figure 4a [187,188]. It requires three Raman beams, two of which are the chirped beams blue and red detuned to the upper energy level. The scanning directions of the two light beams are opposite, and the interference path is completely symmetrical, which can reduce the error caused by the gravity gradient. Since the atoms in the different trajectories are in the same energy level, it is also insensitive to the magnetic field and AC Stark effect. In 2015, Zhou et al. applied this technology to a dual-species atom interferometer and implemented a four-wave double-diffraction Raman transition (FWDR) method for the WEP test [82]. The principle of the FWDR atom interferometer is shown in Figure 4b, which requires four Raman beams (k_1, k_2, k_3, k_4) to achieve the synchronous differential measurement of the dual-species atom interference. k_1 and k_2 together with k_3 interaction with ^{85}Rb, while k_1 and k_2 together with k_4 interaction with ^{87}Rb. This scheme will greatly reduce influence from the laser phase noise and Stark and Zeeman shifts. To suppress the vibration noise of the platform, Bayesian statistical methods are introduced to extract the acceleration difference in a common-mode noise immune way by taking advantage of phase-correlated measurements [154,155]. For the dual-species WEP test, the Hu group applied the fringe-locking method, which fixes the phase measurement invariably at the midfringe [189]. This method extracts the gravity differential phase without bias and effectively suppresses common-mode vibration noise.
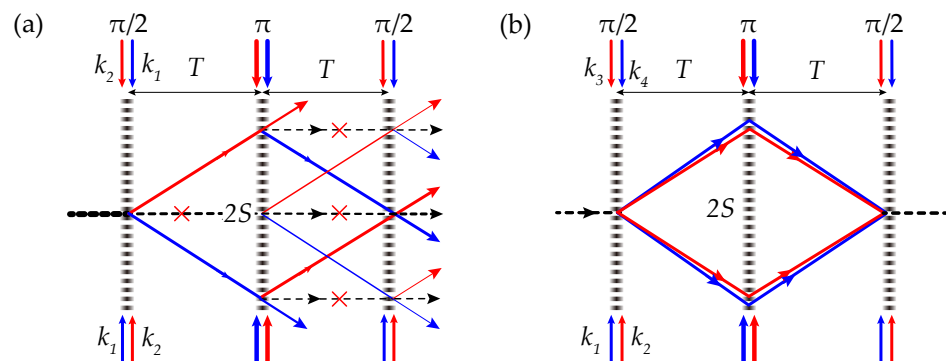

Figure 4. Schematic of double-diffraction Raman transition (**a**) and four-wave double-diffraction Raman transition (**b**). k_1, k_2, k_3 and k_4 are wave vectors of the Raman beams, T is the free evolution time, and $2S$ is the enclosed area of the interference.

4.5. Integrated Packages

Although atom interferometers are typically implemented in ground laboratories, current efforts aim to develop various system packages that are compatible with system integration and modularity for space missions [190,191] and with the size, weight, power consumption and robustness required for the commercial scenarios. Examples are the portable magneto-optical trap system [192], titanium vacuum package [193], laser system package [194] and cold atom physics package [195]. We are not discussing the details here.

5. Prospect and Conclusions

Current accuracy of the WEP tests with atoms has reached the level of 10^{-12} [120], and no violation is observed. To test the WEP with a higher accuracy in the future, we need to improve the sensitivity and accuracy of the atom interferometers. According to Equation (5), there are two major ways to improve the sensitivity: (i) to increase the evolution time T and

(ii) to enlarge the momentum splitting k. A long-baseline setup, microgravity environment or a set of optical lattice can be used to increase the evolution time T. The main method of enlarging k is to use the Bragg diffraction. The research on the influence of the temperature and the entanglement on the sensitivity is reviewed and considered in this section.

Projects on the long-baseline atom interferometer have been proposed and carried out. Hartwig et al. proposed a large baseline atom interferometer test of the WEP with rubidium and ytterbium extending over 10 m of free fall, which could theoretically reach an accuracy in the Eötvös parameter of 7×10^{-13} [127]. The atom interferometer build by the Kasevich group achieved an effective interference length of 8.2 m and an interrogation time $2T$ of 2.3 s [104,196]. They also proposed to establish a 100 m atom interferometer [34]. The Zhan group also realized a 10 m long-baseline atom interferometer towards the verification of the WEP [105,197]. In 2020, they proposed the ZAIGA plan to build a 300 m atom interferometer, which is expected to achieve a maximum integration time of 7.7 s and precision of 10^{-15} for the WEP test [198].

Compared with a free-fall atom interferometer in the gravity field of the Earth, a microgravity environment allows longer evolution time within a short distance, which is more promising for high accuracy tests of the WEP [199,200]. There are several methods to obtain the microgravity environment, including the free-drop tower [201], the parabolic aircraft flight [202,203] and satellite and space station [204,205]. In 2010, research groups in Europe proposed the QUANTUS plan for the WEP test [199,206]. The falling-tower spacecraft operates in both falling and ejection modes, achieving a free-fall duration of 4.7 s and 9.4 s, respectively. In 2009, the Bouyer group proposed to verify the WEP with atoms of ^{87}Rb and ^{40}K during the parabolic flight of an aircraft, which can provide a free-fall duration of up to 20 s [155]. Their experiment was carried out in 2006 with the measured Eötvös parameter of 10^{-4} level under a 0 g environment [114]. Space missions such as the STE-QUEST plan [129,204] and the QTEST plan [130] are proposed, aiming at an accuracy of 10^{-15} in the WEP test. The Cold Atom Lab (CAL) in the International Space Station was first powered operated in 2018, and the ^{87}Rb ultracold BEC was prepared on board [207]. Last year, the microgravity scientific laboratory cabinet (MSLC) was launched to the China Space Station with the aim of testing the WEP in the level of 10^{-10} [208]. One can find more experimental details on the microgravity environment in space in [209].

The third idea to prolong the evolution time is the Bloch oscillation, which can hold atoms in the optical lattice. In 2019, the Müller group suspended the spatially separated atomic wave packet for up to 20 s by an lattice formed in an optical cavity [81]. This new interferometer design is promising to achieve the high accuracy in the WEP test within a compact volume in the future.

Another way to improve the sensitivity of the atom interferometer is to achieve LMT of atoms, which can be realized using Bragg diffraction. In 2008, the Müller group achieved a breakthrough in 24-photon-momentum beam splitting of the thermal cold atom ensemble using Bragg diffraction [134]. The Kasevich group achieved momentum transfer of 102 photons using sequential multiphoton Bragg diffraction in BEC [210]. In 2018, the Gupta group achieved a maximum of 112 photon momentum transfer, with an interference contrast of up to 30% [211]. However, no experiment using the Bragg-diffraction atom interferometers has shown any better sensitivity in gravity measurement than the ordinary Raman-pulse scheme by now. This is mainly due to the low efficiency of the atomic momentum transfer and the low contrast of the final interference fringe in the LMT-based scheme.

In addition, the atomic temperature can also influence the sensitivity of the WEP test because the expansion of atoms can limit the atomic free-fall time and recombination of the atomic wave packets. Thus, we need to reduce the atomic temperature as low as possible to reduce the expansion of atoms. We can tune the atom–atom interactions to prepare the ultracold BEC atoms [212]. However, the low temperature will result in a limited atom number with large shot noise. In the experiment, we need a large number of atoms to benefit the signal-to-noise ratio of the atom interferometer. Thus, we need to make a

balance between avoiding the expansion of atoms and capturing more atoms to increase the signal-to-noise ratio so that we can prepare more atoms within a shorter cycle time, which is an important task in the future.

On the other hand, in the existence of the entanglement, the measurement accuracy can beat the standard quantum limit $1/\sqrt{N}$ and approach the Heisenberg limit $1/N$ in quantum metrology [213]. Since the number of atoms cannot increase infinitely, preparing nonclassical states of the atoms for the future verification of the WEP will be one promising solution. In 2021, Anders et al. implemented momentum-entangled atoms with a squeezing parameter of (-3.1 ± 0.8) dB that is compatible with atom interferometers [214]. Though it is challenging to build up an entanglement-enhanced atom interferometer, unprecedented sensitivities for gravity measurement are very attractive [214]. Additionally, although there is no theoretical model to predict the WEP violation in the presence of entanglement, the entanglement involved in the atom interferometer and the WEP test will allow us to check possible quantum version of gravity, leading to better understanding of space–time and nonlocality [63]. In 2018, Geiger and Truple proposed a quantum test of the WEP with entangled atoms of ^{85}Rb and ^{87}Rb in a high-finesse cavity [83]. Last year, Overstreet et al. measured the gravitational Aharonov–Bohm effect by placing a kilogram-scale source mass close to one of the atomic wave packets in an LMT-based atom interferometer [215]. We expect more theories and experiments in the near future can help us understand better about entanglement and gravity and the interplay between them.

In summary, the WEP test with cold atoms provides us an opportunity to search for any evidence of the violation of the GR theory, where both quantum and gravity emerge. With current accuracy of the WEP test using the macroscopic and microscopic objects reaching the level of 10^{-15} [26,27] and 10^{-12} [120], respectively, we still have not observed any signs of the WEP breaking. However, as seen in this review, the potential advantages of using cold atoms to verify WEP have not been fully explored. Pushing the limits of the accuracy to higher levels with various microscopic atoms is the major research goal of the WEP test, though plenty of challenges and problems must be addressed [216]. Firstly, although WEP test experiments using non-isotopes may be more attractive [126,217], the experimental accuracy of WEP verification for non-isotopic atoms is generally low at present [112–116]. The main challenge is the difficulty in correcting system errors caused by different effective wave vectors for different atoms. Feasible methods are converting these noises into common-mode noise and reducing atom temperature to improve verification accuracy. Secondly, in a long-baseline atom interferometer, the error induced by the gravity gradient is a systematic error that is difficult to ignore due to the long distance of atoms falling. In addition to utilizing the method of Section 4 to reduce the error induced by gravity gradients, LMT technology and microgravity environments can also be developed to reduce the impact of gravity gradients and improve validation accuracy. Thirdly, the WEP test using large-scale molecules is still at its initial stage [96]. In its development, the corresponding cooling methods should be urgently put at the first priority. In the future, the controlling techniques of the multiple degrees of freedom, such as the chirality, the internal states and composition of different molecules, may also need to be developed in the large-scale WEP test using molecules. And what is more interesting and challenging in future WEP experiment tests is to use nonlocal correlations of atoms, such as atomic entanglement and squeezing [83–85,87]. Currently, there are relatively few experiments in this field, but it is potentially worthwhile to find possible evidence of the influence of entanglement in gravity. Also, further validation of LPI and LLI can be achieved using cold atoms, and some proposals and experiments have been proposed [218–224]. We believe future stringent tests of the WEP will open new doors to physics, such as modifying the GR theory, establishing a quantum gravity theory and searching for new forces or matter.

Data Availability Statement: No new data were created or analyzed in this study. Data sharing is not applicable to this article.

Conflicts of Interest: The authors declare no conflict of interest.

Abbreviations

The following abbreviations are used in this manuscript:

Acronym	Meaning	Section
AI	atom interferometry	2
AOM	acousto-optic modulation	4
BEC	Bose–Einstein condensate	4, 5
CAL	Cold Atom Lab	5
EEP	Einstein equivalence principle	1
EOM	electro-optic modulation	4
FWDR	four-wave double-diffraction Raman transition	3, 4
GR	general relativity	1, 5
HUST	Huazhong University of Science and Technology	3, 4
I/Q	in-phase/quadrature	4
LLI	local Lorentz invariance	1, 5
LMT	large momentum transfer	4, 5
LPI	local position invariance	1, 5
LP2N	The Photonics, Numerical and Nanosciences Laboratory	3
LUH	Leibniz Universität Hannover	3
LENS	European Laboratory for Non Linear Spectroscopy	3
MICROSCOPE	Micro-Satellite a traînée Compensée pour l'Observation du Principe d'Equivalence	1
MPIQ	Max-Planck-Institut für Quantenoptik	3
MSLC	microgravity scientific laboratory cabinet	5
OPLL	optical phase lock-loop	4
ONERA	The French Aerospace Lab	3, 5
QTEST	Quantum Test of the Equivalence Principle in Space	5
QUANTUS	QUANTen Gase Unter Schwerelosigkeit	5
SM	Standard Model	1
STE-QUEST	Space–Time Explorer and Quantum Equivalence principle Space Test	5
UFF	University of Free Fall	1
WEP	weak equivalence principle	1, 2, 3, 4, 5
WIPM	Wuhan Institute of Physics and Mathematics	3, 4
ZAIGA	The Zhaoshan Long-Baseline Atom Interferometer Gravitation Antenna	5

References

1. Kragh, H.; Smith, R.W. Who discovered the expanding universe? *Hist. Sci.* **2003**, *41*, 141–162. [CrossRef]
2. Ade, P.A.; Aghanim, N.; Alves, M.; Armitage-Caplan, C.; Arnaud, M.; Ashdown, M.; Atrio-Barandela, F.; Aumont, J.; Aussel, H.; Baccigalupi, C.; et al. Planck 2013 results. I. Overview of products and scientific results. *Astron. Astrophys.* **2014**, *571*, A1. [CrossRef]
3. Bell, J.S. On the Problem of Hidden Variables in Quantum Mechanics. *Rev. Mod. Phys.* **1966**, *38*, 447–452. [CrossRef]
4. Bell, J.S. On the Einstein Podolsky Rosen paradox. *Phys. Phys. Fiz.* **1964**, *1*, 195–200. [CrossRef]
5. Aspect, A.; Dalibard, J.; Roger, G. Experimental Test of Bell's Inequalities Using Time-Varying Analyzers. *Phys. Rev. Lett.* **1982**, *49*, 1804–1807. [CrossRef]

6. Amico, L.; Fazio, R.; Osterloh, A.; Vedral, V. Entanglement in many-body systems. *Rev. Mod. Phys.* **2008**, *80*, 517–576. [CrossRef]
7. Mintert, F.; Kuś, M.; Buchleitner, A. Concurrence of Mixed Multipartite Quantum States. *Phys. Rev. Lett.* **2005**, *95*, 260502. [CrossRef]
8. Yang, C.N.; Mills, R.L. Conservation of Isotopic Spin and Isotopic Gauge Invariance. *Phys. Rev.* **1954**, *96*, 191–195. [CrossRef]
9. Dicke, R. Republication of: The theoretical significance of experimental relativity. *Gen. Relativ. Gravit.* **2019**, *51*, 1–31. [CrossRef]
10. Whitrow, G.J. Gravitation and Cosmology: Principles and Applications of the General Theory of Relativity. *Phys. Bull.* **1974**, *25*, 65. [CrossRef]
11. Brans, C.; Dicke, R.H. Mach's Principle and a Relativistic Theory of Gravitation. *Phys. Rev.* **1961**, *124*, 925–935. [CrossRef]
12. Will, C.M. *Theory and Experiment in Gravitational Physics*; Cambridge University: Cambridge, UK, 2018.
13. Ciufolini, I.; Wheeler, J.A. *Gravitation and Inertia*; Princeton University Press: Princeton, NJ, USA, 1995; Volume 101.
14. Damour, T.; Polyakov, A.M. String theory and gravity. *Gen. Relativ. Gravit.* **1994**, *26*, 1171–1176. [CrossRef]
15. Scherk, J.; Schwarz, J. Dual models and the geometry of space-time. *Phys. Lett. B* **1974**, *52*, 347–350. [CrossRef]
16. Chiou, D.W. Loop quantum gravity. *Int. J. Mod. Phys. D* **2015**, *24*, 1530005. [CrossRef]
17. Kostelecký, V.A. Gravity, Lorentz violation, and the standard model. *Phys. Rev. D* **2004**, *69*, 105009. [CrossRef]
18. Damour, T. Theoretical aspects of the equivalence principle. *Class. Quantum Gravity* **2012**, *29*, 184001. [CrossRef]
19. Fayet, P. A new long-range force? *Phys. Lett. B* **1986**, *171*, 261–266. [CrossRef]
20. Fayet, P. The fifth interaction in grand-unified theories: A new force acting mostly on neutrons and particle spins. *Phys. Lett. B* **1986**, *172*, 363–368. [CrossRef]
21. Dimopoulos, S.; Graham, P.W.; Hogan, J.M.; Kasevich, M.A. General relativistic effects in atom interferometry. *Phys. Rev. D* **2008**, *78*, 042003. [CrossRef]
22. Graham, P.W.; Kaplan, D.E.; Mardon, J.; Rajendran, S.; Terrano, W.A. Dark matter direct detection with accelerometers. *Phys. Rev. D* **2016**, *93*, 075029. [CrossRef]
23. Hees, A.; Minazzoli, O.; Savalle, E.; Stadnik, Y.V.; Wolf, P. Violation of the equivalence principle from light scalar dark matter. *Phys. Rev. D* **2018**, *98*, 064051. [CrossRef]
24. Sondag, A.; Dittus, H. Electrostatic Positioning System for a free fall test at drop tower Bremen and an overview of tests for the Weak Equivalence Principle in past, present and future. *Adv. Space Res.* **2016**, *58*, 644–677. [CrossRef]
25. Potter, H.H.; Richardson, O.W. Some experiments on the proportionality of mass and weight. *Proc. R. Soc. Lond. Ser. A* **1923**, *104*, 588–610. [CrossRef]
26. Carusotto, S.; Cavasinni, V.; Mordacci, A.; Perrone, F.; Polacco, E.; Iacopini, E.; Stefanini, G. Test of g universality with a Galileo type experiment. *Phys. Rev. Lett.* **1992**, *69*, 1722–1725. [CrossRef] [PubMed]
27. Carusotto, S.; Cavasinni, V.; Perrone, F.; Polacco, E.; Iacopini, E.; Stefanini, G. g-Universality test with a Galileo's type experiment. *Nuov. Cim. B* **1996**, *111*, 1259–1275. [CrossRef]
28. Schlamminger, S.; Choi, K.Y.; Wagner, T.A.; Gundlach, J.H.; Adelberger, E.G. Test of the Equivalence Principle Using a Rotating Torsion Balance. *Phys. Rev. Lett.* **2008**, *100*, 041101. [CrossRef]
29. Zhu, L.; Liu, Q.; Zhao, H.H.; Gong, Q.L.; Yang, S.Q.; Luo, P.; Shao, C.G.; Wang, Q.L.; Tu, L.C.; Luo, J. Test of the Equivalence Principle with Chiral Masses Using a Rotating Torsion Pendulum. *Phys. Rev. Lett.* **2018**, *121*, 261101. [CrossRef]
30. Viswanathan, V.; Fienga, A.; Minazzoli, O.; Bernus, L.; Laskar, J.; Gastineau, M. The new lunar ephemeris INPOP17a and its application to fundamental physics. *Mon. Not. R. Astron. Soc.* **2018**, *476*, 1877–1888. [CrossRef]
31. Hofmann, F.; Müller, J. Relativistic tests with lunar laser ranging. *Class. Quantum Gravity* **2018**, *35*, 035015. [CrossRef]
32. Touboul, P.; Métris, G.; Rodrigues, M.; Bergé, J.; Robert, A.; Baghi, Q.; André, Y.; Bedouet, J.; Boulanger, D.; Bremer, S.; et al. *MICROSCOPE* Mission: Final Results of the Test of the Equivalence Principle. *Phys. Rev. Lett.* **2022**, *129*, 121102. [CrossRef]
33. Touboul, P.; Métris, G.; Rodrigues, M.; Bergé, J.; Robert, A.; Baghi, Q.; André, Y.; Bedouet, J.; Boulanger, D.; Bremer, S.; et al. Result of the MICROSCOPE weak equivalence principle test. *Class. Quantum Gravity* **2022**, *39*, 204009. [CrossRef]
34. Dimopoulos, S.; Graham, P.W.; Hogan, J.M.; Kasevich, M.A. Testing General Relativity with Atom Interferometry. *Phys. Rev. Lett.* **2007**, *98*, 111102. [CrossRef] [PubMed]
35. Miffre, A.; Jacquey, M.; Büchner, M.; Trénec, G.; Vigué, J. Atom interferometry. *Phys. Scr.* **2006**, *74*, C15. [CrossRef]
36. Khoury, J. Chameleon field theories. *Class. Quantum Gravity* **2013**, *30*, 214004. [CrossRef]
37. Burrage, C.; Copeland, E.J.; Hinds, E. Probing dark energy with atom interferometry. *J. Cosmol. Astropart. Phys.* **2015**, *2015*, 042. [CrossRef]
38. Hamilton, P.; Jaffe, M.; Haslinger, P.; Simmons, Q.; Müller, H.; Khoury, J. Atom-interferometry constraints on dark energy. *Science* **2015**, *349*, 849–851.
39. Burrage, C.; Copeland, E.J. Using atom interferometry to detect dark energy. *Contemp. Phys.* **2016**, *57*, 164–176.
40. Elder, B.; Khoury, J.; Haslinger, P.; Jaffe, M.; Müller, H.; Hamilton, P. Chameleon dark energy and atom interferometry. *Phys. Rev. D* **2016**, *94*, 044051. [CrossRef]
41. Puetzfeld, D.; Obukhov, Y.N. Propagation equations for deformable test bodies with microstructure in extended theories of gravity. *Phys. Rev. D* **2007**, *76*, 084025. [CrossRef]
42. Yasskin, P.B.; Stoeger, W.R. Propagation equations for test bodies with spin and rotation in theories of gravity with torsion. *Phys. Rev. D* **1980**, *21*, 2081–2094. [CrossRef]

43. Hehl, F.W.; von der Heyde, P.; Kerlick, G.D.; Nester, J.M. General relativity with spin and torsion: Foundations and prospects. *Rev. Mod. Phys.* **1976**, *48*, 393–416. [CrossRef]

44. Shapiro, I. Physical aspects of the space–time torsion. *Phys. Rep.* **2002**, *357*, 113–213. [CrossRef]

45. Obukhov, Y.N.; Silenko, A.J.; Teryaev, O.V. Spin-torsion coupling and gravitational moments of Dirac fermions: Theory and experimental bounds. *Phys. Rev. D* **2014**, *90*, 124068. [CrossRef]

46. Hammond, R.T. Torsion gravity. *Rep. Prog. Phys.* **2002**, *65*, 599. [CrossRef]

47. Bong, K.; Holynski, M.; Vovrosh, J.; Bouyer, P.; Condon, G.; Rasel, E.; Schubert, C.; Schleich, W.P.; Roura, A. Taking atom interferometric quantum sensors from the laboratory to real-world applications. *Nat. Rev. Phys.* **2019**, *1*, 731–739. [CrossRef]

48. Geiger, R.; Landragin, A.; Merlet, S.; Pereira Dos Santos, F. High-accuracy inertial measurements with cold-atom sensors. *AVS Quantum Sci.* **2020**, *2*, 024702. [CrossRef]

49. Nabighian, M.N.; Ander, M.E.; Grauch, V.J.S.; Hansen, R.O.; LaFehr, T.R.; Li, Y.; Pearson, W.C.; Peirce, J.W.; Phillips, J.D.; Ruder, M.E. Historical development of gravity method in exploration. *Geophysics* **2005**, *70*, 63ND–89ND. [CrossRef]

50. Bidel, Y.; Zahzam, N.; Blanchard, C.; Bonnin, A.; Cadoret, M.; Bresson, A.; Rouxel, D.; Lequentrec-Lalancette, M.F. Absolute marine gravimetry with matter-wave interferometry. *Nat. Commun.* **2018**, *9*, 627. [CrossRef]

51. Bidel, Y.; Zahzam, N.; Bresson, A.; Blanchard, C.; Cadoret, M.; Olesen, V.A.; Forsberg, R. Absolute airborne gravimetry with a cold atom sensor. *J. Geod.* **2020**, *94*, 20. [CrossRef]

52. Boddice, D.; Metje, N.; Tuckwell, G. Capability assessment and challenges for quantum technology gravity sensors for near surface terrestrial geophysical surveying. *J. Appl. Geophy* **2017**, *146*, 149–159. [CrossRef]

53. Stray, B.; Lamb, A.; Kaushik, A.; Vovrosh, J.; Rodgers, A.; Winch, J.; Hayati, F.; Boddice, D.; Stabrawa, A.; Niggebaum, A.; et al. Quantum sensing for gravity cartography. *Nature* **2022**, *602*, 590–594. [CrossRef] [PubMed]

54. Jiang, Z.; Pálinkáš, V.; Arias, F.E.; Liard, J.; Merlet, S.; Wilmes, H.; Vitushkin, L.; Robertsson, L.; Tisserand, L.; Santos, F.P.D.; et al. The 8th International Comparison of Absolute Gravimeters 2009: The first Key Comparison (CCM.G-K1) in the field of absolute gravimetry. *Metrologia* **2012**, *49*, 666. [CrossRef]

55. Stock, M.; Davis, R.; de Mirandés, E.; Milton, M.J.T. The revision of the SI—the result of three decades of progress in metrology. *Metrologia* **2019**, *56*, 022001. [CrossRef]

56. Wu, S.; Feng, J.; Li, C.; Su, D.; Wang, Q.; Hu, R.; Mou, L. The results of 10th International Comparison of Absolute Gravimeters (ICAG-2017). *J. Geod.* **2021**, *95*, 63. [CrossRef]

57. Rosi, G.; Sorrentino, F.; Cacciapuoti, L.; Prevedelli, M.; Tino, G.M. Precision measurement of the Newtonian gravitational constant using cold atoms. *Nature* **2014**, *510*, 518–521. [CrossRef]

58. Fixler, J.B.; Foster, G.T.; McGuirk, J.M.; Kasevich, M.A. Atom Interferometer Measurement of the Newtonian Constant of Gravity. *Science* **2007**, *315*, 74–77. [CrossRef]

59. Bouchendira, R.; Cladé, P.; Guellati-Khélifa, S.; Nez, F.; Biraben, F. New Determination of the Fine Structure Constant and Test of the Quantum Electrodynamics. *Phys. Rev. Lett.* **2011**, *106*, 080801. [CrossRef]

60. Parker, R.H.; Yu, C.; Zhong, W.; Estey, B.; Müller, H. Measurement of the fine-structure constant as a test of the Standard Model. *Science* **2018**, *360*, 191–195. [CrossRef]

61. Morel, L.; Yao, Z.; Clade, P.; Guellati-Khelifa, S. Determination of the fine-structure constant with an accuracy of 81 parts per trillion. *Nature* **2020**, *588*, 61–65. [CrossRef]

62. Herrmann, S.; Dittus, H.; Lämmerzahl, C.; (for the QUANTUS and PRIMUS teams). Testing the equivalence principle with atomic interferometry. *Class. Quantum Gravity* **2012**, *29*, 184003. [CrossRef]

63. Tino, G.; Cacciapuoti, L.; Capozziello, S.; Lambiase, G.; Sorrentino, F. Precision gravity tests and the Einstein Equivalence Principle. *Prog. Part. Nucl. Phys.* **2020**, *112*, 103772. [CrossRef]

64. Tino, G.M. Testing gravity with cold atom interferometry: Results and prospects. *Quantum Sci. Technol.* **2021**, *6*, 024014. [CrossRef]

65. Hohensee, M.; Lan, S.Y.; Houtz, R.; Chan, C.; Estey, B.; Kim, G.; Kuan, P.C.; Müller, H. Sources and technology for an atomic gravitational wave interferometric sensor. *Gen. Relativ. Gravit.* **2011**, *43*, 1905–1930. [CrossRef]

66. Graham, P.W.; Hogan, J.M.; Kasevich, M.A.; Rajendran, S. New Method for Gravitational Wave Detection with Atomic Sensors. *Phys. Rev. Lett.* **2013**, *110*, 171102. [CrossRef]

67. Wang, Y.J.; Lu, X.Y.; Qin, C.G.; Tan, Y.J.; Shao, C.G. Modeling gravitational wave detection with atom interferometry. *Class. Quantum Gravity* **2021**, *38*, 145025. [CrossRef]

68. Will, C.M. The confrontation between general relativity and experiment. *Living Rev. Relativ.* **2014**, *17*, 4. [CrossRef]

69. Moosbrugger, D. An Update on the Impact of Schiff's Conjecture on Tests of the Einstein Equivalence Principle Today. Master's Thesis, ETH Zürich, Zürich, Switzerland, 2018.

70. Peters, A.; Chung, K.Y.; Chu, S. High-precision gravity measurements using atom interferometry. *Metrologia* **2001**, *38*, 25–61. [CrossRef]

71. Giltner, D.M.; McGowan, R.W.; Lee, S.A. Atom Interferometer Based on Bragg Scattering from Standing Light Waves. *Phys. Rev. Lett.* **1995**, *75*, 2638–2641. [CrossRef]

72. Siemß, J.N.; Fitzek, F.; Abend, S.; Rasel, E.M.; Gaaloul, N.; Hammerer, K. Analytic theory for Bragg atom interferometry based on the adiabatic theorem. *Phys. Rev. A* **2020**, *102*, 033709. [CrossRef]

73. Béguin, A.; Rodzinka, T.; Vigué, J.; Allard, B.; Gauguet, A. Characterization of an atom interferometer in the quasi-Bragg regime. *Phys. Rev. A* **2022**, *105*, 033302. [CrossRef]

74. Cladé, P.; Guellati-Khélifa, S.; Nez, F.; Biraben, F. Large Momentum Beam Splitter Using Bloch Oscillations. *Phys. Rev. Lett.* **2009**, *102*, 240402. [CrossRef] [PubMed]

75. Müller, H.; Chiow, S.; Herrmann, S.; Chu, S. Atom Interferometers with Scalable Enclosed Area. *Phys. Rev. Lett.* **2009**, *102*, 240403. [CrossRef]

76. McAlpine, K.E.; Gochnauer, D.; Gupta, S. Excited-band Bloch oscillations for precision atom interferometry. *Phys. Rev. A* **2020**, *101*, 023614. [CrossRef]

77. Poli, N.; Wang, F.Y.; Tarallo, M.G.; Alberti, A.; Prevedelli, M.; Tino, G.M. Precision Measurement of Gravity with Cold Atoms in an Optical Lattice and Comparison with a Classical Gravimeter. *Phys. Rev. Lett.* **2011**, *106*, 038501. [CrossRef] [PubMed]

78. Charrière, R.; Cadoret, M.; Zahzam, N.; Bidel, Y.; Bresson, A. Local gravity measurement with the combination of atom interferometry and Bloch oscillations. *Phys. Rev. A* **2012**, *85*, 013639. [CrossRef]

79. Dunning, A.; Gregory, R.; Bateman, J.; Cooper, N.; Himsworth, M.; Jones, J.A.; Freegarde, T. Composite pulses for interferometry in a thermal cold atom cloud. *Phys. Rev. A* **2014**, *90*, 033608. [CrossRef]

80. Berg, P.; Abend, S.; Tackmann, G.; Schubert, C.; Giese, E.; Schleich, W.P.; Narducci, F.A.; Ertmer, W.; Rasel, E.M. Composite-Light-Pulse Technique for High-Precision Atom Interferometry. *Phys. Rev. Lett.* **2015**, *114*, 063002. [CrossRef]

81. Xu, V.; Jaffe, M.; Panda, C.D.; Kristensen, S.L.; Clark, L.W.; Müller, H. Probing gravity by holding atoms for 20 seconds. *Science* **2019**, *366*, 745–749. [CrossRef]

82. Zhou, L.; Long, S.; Tang, B.; Chen, X.; Gao, F.; Peng, W.; Duan, W.; Zhong, J.; Xiong, Z.; Wang, J.; et al. Test of Equivalence Principle at 10^{-8} Level by a Dual-Species Double-Diffraction Raman Atom Interferometer. *Phys. Rev. Lett.* **2015**, *115*, 013004. [CrossRef]

83. Geiger, R.; Trupke, M. Proposal for a Quantum Test of the Weak Equivalence Principle with Entangled Atomic Species. *Phys. Rev. Lett.* **2018**, *120*, 043602. [CrossRef]

84. Viola, L.; Onofrio, R. Testing the equivalence principle through freely falling quantum objects. *Phys. Rev. D* **1997**, *55*, 455–462. [CrossRef]

85. Kajari, E.; Harshman, N.; Rasel, E.; Stenholm, S.; Süssmann, G.; Schleich, W.P. Inertial and gravitational mass in quantum mechanics. *Appl. Phys. B* **2010**, *100*, 43–60. [CrossRef]

86. Orlando, P.J.; Mann, R.B.; Modi, K.; Pollock, F.A. A test of the equivalence principle(s) for quantum superpositions. *Class. Quantum Gravity* **2016**, *33*, 19LT01. [CrossRef]

87. Zych, M.; Brukner, C. Quantum formulation of the Einstein equivalence principle. *Nat. Phys.* **2018**, *14*, 1027–1031. [CrossRef]

88. Chu, S.; Hollberg, L.; Bjorkholm, J.E.; Cable, A.; Ashkin, A. Three-dimensional viscous confinement and cooling of atoms by resonance radiation pressure. *Phys. Rev. Lett.* **1985**, *55*, 48–51. [CrossRef] [PubMed]

89. Lett, P.D.; Watts, R.N.; Westbrook, C.I.; Phillips, W.D.; Gould, P.L.; Metcalf, H.J. Observation of Atoms Laser Cooled below the Doppler Limit. *Phys. Rev. Lett.* **1988**, *61*, 169–172. [CrossRef]

90. Aspect, A.; Arimondo, E.; Kaiser, R.; Vansteenkiste, N.; Cohen-Tannoudji, C. Laser Cooling below the One-Photon Recoil Energy by Velocity-Selective Coherent Population Trapping. *Phys. Rev. Lett.* **1988**, *61*, 826–829. [CrossRef] [PubMed]

91. Kasevich, M.; Chu, S. Atomic interferometry using stimulated Raman transitions. *Phys. Rev. Lett.* **1991**, *67*, 181–184. [CrossRef]

92. Peters, A.; Chung, K.; Chu, S. Measurement of gravitational acceleration by dropping atoms. *Nature* **1999**, *400*, 849–852. [CrossRef]

93. Clauser, J.F. Ultra-high sensitivity accelerometers and gyroscopes using neutral atom matter-wave interferometry. *Physica B+C* **1988**, *151*, 262–272. [CrossRef]

94. Walz, J.; Hansch, T. A proposal to measure antimatter gravity using ultracold antihydrogen atoms. *Gen. Relativ. Gravity* **2004**, *36*, 561–570. [CrossRef]

95. Hamilton, P.; Zhmoginov, A.; Robicheaux, F.; Fajans, J.; Wurtele, J.S.; Müller, H. Antimatter Interferometry for Gravity Measurements. *Phys. Rev. Lett.* **2014**, *112*, 121102. [CrossRef]

96. Rodewald, J.; Dörre, N.; Grimaldi, A.; Geyer, P.; Felix, L.; Mayor, M.; Shayeghi, A.; Arndt, M. Isotope-selective high-order interferometry with large organic molecules in free fall. *New J. Phys.* **2018**, *20*, 033016. [CrossRef]

97. Amoretti, M.; Amsler, C.; Bonomi, G.; Bouchta, A.; Bowe, P.; Carraro, C.; Cesar, C.; Charlton, M.; Collier, M.; Doser, M.; et al. Production and detection of cold antihydrogen atoms. *Nature* **2002**, *419*, 456–459. [CrossRef] [PubMed]

98. Baker, C.J.; Bertsche, W.; Capra, A.; Cesar, C.L.; Charlton, M.; Mathad, A.C.; Eriksson, S.; Evans, A.; Evetts, N.; Fabbri, S.; et al. Sympathetic cooling of positrons to cryogenic temperatures for antihydrogen production. *Nat. Commun.* **2021**, *12*, 6139. [CrossRef]

99. Pedalino, S.; Galindo, B.R.; de Sousa, T.; Fein, Y.Y.; Geyer, P.; Gerlich, S.; Arndt, M. Experimental challenges for high-mass matter-wave interference with nanoparticles. In *Proceedings of the Quantum Sensing, Imaging, and Precision Metrology*; Scheuer, J., Shahriar, S.M., Eds.; International Society for Optics and Photonics; SPIE: Bellingham, WA, USA, 2023; Volume 12447, p. 124470K. [CrossRef]

100. Fray, S.; Diez, C.A.; Hänsch, T.W.; Weitz, M. Atomic Interferometer with Amplitude Gratings of Light and Its Applications to Atom Based Tests of the Equivalence Principle. *Phys. Rev. Lett.* **2004**, *93*, 240404. [CrossRef]

101. Altin, P.A.; Johnsson, M.T.; Negnevitsky, V.; Dennis, G.R.; Anderson, R.P.; Debs, J.E.; Szigeti, S.S.; Hardman, K.S.; Bennetts, S.; McDonald, G.D.; et al. Precision atomic gravimeter based on Bragg diffraction. *New J. Phys.* **2013**, *15*, 023009. [CrossRef]

102. Wu, B.; Wang, Z.; Cheng, B.; Wang, Q.; Xu, A.; Lin, Q. The investigation of a µGal-level cold atom gravimeter for field applications. *Metrologia* **2014**, *51*, 452–458. [CrossRef]

103. Zhou, L.; Xiong, Z.Y.; Yang, W.; Tang, B.; Peng, W.C.; Wang, Y.B.; Xu, P.; Wang, J.; Zhan, M.S. Measurement of local gravity via a cold atom interferometer. *Chin. Phys. Lett.* **2011**, *28*, 013701. [CrossRef]

104. Dickerson, S.M.; Hogan, J.M.; Sugarbaker, A.; Johnson, D.M.S.; Kasevich, M.A. Multiaxis Inertial Sensing with Long-Time Point Source Atom Interferometry. *Phys. Rev. Lett.* **2013**, *111*, 083001. [CrossRef]

105. Zhou, L.; Yan, S.T.; Ji, Y.H.; He, C.; Jiang, J.J.; Hou, Z.; Xu, R.D.; Wang, Q.; Li, Z.X.; Gao, D.F.; et al. Toward a high-precision mass–energy test of the equivalence principle with atom interferometers. *Front. Phys.* **2022**, *10*, 1039119. [CrossRef]

106. Bodart, Q.; Merlet, S.; Malossi, N.; Dos Santos, F.P.; Bouyer, P.; Landragin, A. A cold atom pyramidal gravimeter with a single laser beam. *Appl. Phys. Lett.* **2010**, *96*, 134101. [CrossRef]

107. Bidel, Y.; Carraz, O.; Charrière, R.; Cadoret, M.; Zahzam, N.; Bresson, A. Compact cold atom gravimeter for field applications. *Appl. Phys. Lett.* **2013**, *102*, 144107. [CrossRef]

108. Hauth, M.; Freier, C.; Schkolnik, V.; Senger, A.; Schmidt, M.; Peters, A. First gravity measurements using the mobile atom interferometer GAIN. *Appl. Phys. B* **2013**, *113*, 49–55. [CrossRef]

109. Wang, S.K.; Zhao, Y.; Zhuang, W.; Li, T.C.; Wu, S.Q.; Feng, J.Y.; Li, C.J. Shift evaluation of the atomic gravimeter NIM-AGRb-1 and its comparison with FG5X. *Metrologia* **2018**, *55*, 360–365. [CrossRef]

110. Huang, P.W.; Tang, B.; Chen, X.; Zhong, J.Q.; Xiong, Z.Y.; Zhou, L.; Wang, J.; Zhan, M.S. Accuracy and stability evaluation of the ^{85} Rb atom gravimeter WAG-H5-1 at the 2017 International Comparison of Absolute Gravimeters. *Metrologia* **2019**, *56*, 045012. [CrossRef]

111. Fu, Z.; Wu, B.; Cheng, B.; Zhou, Y.; Weng, K.; Zhu, D.; Wang, Z.; Lin, Q. A new type of compact gravimeter for long-term absolute gravity monitoring. *Metrologia* **2019**, *56*, 025001. [CrossRef]

112. Schlippert, D.; Hartwig, J.; Albers, H.; Richardson, L.L.; Schubert, C.; Roura, A.; Schleich, W.P.; Ertmer, W.; Rasel, E.M. Quantum Test of the Universality of Free Fall. *Phys. Rev. Lett.* **2014**, *112*, 203002. [CrossRef]

113. Barrett, B.; Antoni-Micollier, L.; Chichet, L.; Battelier, B.; Gominet, P.A.; Bertoldi, A.; Bouyer, P.; Landragin, A. Correlative methods for dual-species quantum tests of the weak equivalence principle. *New J. Phys.* **2015**, *17*, 085010. [CrossRef]

114. Barrett, B.; Antoni-Micollier, L.; Chichet, L.; Battelier, B.; Leveque, T.; Landragin, A.; Bouyer, P. Dual matter-wave inertial sensors in weightlessness. *Nat. Commun.* **2016**, *7*, 13786. [CrossRef]

115. Albers, H.; Herbst, A.; Richardson, L.L.; Heine, H.; Nath, D.; Hartwig, J.; Schubert, C.; Vogt, C.; Woltmann, M.; Laemmerzahl, C.; et al. Quantum test of the Universality of Free Fall using rubidium and potassium. *Eur. Phys. J. D* **2020**, *74*, 145. [CrossRef]

116. Barrett, B.; Condon, G.; Chichet, L.; Antoni-Micollier, L.; Arguel, R.; Rabault, M.; Pelluet, C.; Jarlaud, V.; Landragin, A.; Bouyer, P.; et al. Testing the universality of free fall using correlated $^{39}K - ^{87}Rb$ atom interferometers. *AVS Quantum Sci.* **2022**, *4*, 014401. [CrossRef]

117. Bonnin, A.; Zahzam, N.; Bidel, Y.; Bresson, A. Simultaneous dual-species matter-wave accelerometer. *Phys. Rev. A* **2013**, *88*, 043615. [CrossRef]

118. Tarallo, M.G.; Mazzoni, T.; Poli, N.; Sutyrin, D.V.; Zhang, X.; Tino, G.M. Test of Einstein Equivalence Principle for 0-Spin and Half-Integer-Spin Atoms: Search for Spin-Gravity Coupling Effects. *Phys. Rev. Lett.* **2014**, *113*, 023005. [CrossRef]

119. Overstreet, C.; Asenbaum, P.; Kovachy, T.; Notermans, R.; Hogan, J.M.; Kasevich, M.A. Effective Inertial Frame in an Atom Interferometric Test of the Equivalence Principle. *Phys. Rev. Lett.* **2018**, *120*, 183604. [CrossRef]

120. Asenbaum, P.; Overstreet, C.; Kim, M.; Curti, J.; Kasevich, M.A. Atom-Interferometric Test of the Equivalence Principle at the 10^{-12} Level. *Phys. Rev. Lett.* **2020**, *125*, 191101. [CrossRef]

121. Zhou, L.; He, C.; Yan, S.T.; Chen, X.; Gao, D.F.; Duan, W.T.; Ji, Y.H.; Xu, R.D.; Tang, B.; Zhou, C.; et al. Joint mass-and-energy test of the equivalence principle at the 10^{-10} level using atoms with specified mass and internal energy. *Phys. Rev. A* **2021**, *104*, 022822. [CrossRef]

122. Duan, X.C.; Deng, X.B.; Zhou, M.K.; Zhang, K.; Xu, W.J.; Xiong, F.; Xu, Y.Y.; Shao, C.G.; Luo, J.; Hu, Z.K. Test of the Universality of Free Fall with Atoms in Different Spin Orientations. *Phys. Rev. Lett.* **2016**, *117*, 023001. [CrossRef]

123. Rosi, G.; D'Amico, G.; Cacciapuoti, L.; Sorrentino, F.; Prevedelli, M.; Zych, M.; Brukner, C.; Tino, G.M. Quantum test of the equivalence principle for atoms in coherent superposition of internal energy states. *Nat. Commun.* **2017**, *8*, 15529. [CrossRef]

124. Zhang, K.; Zhou, M.K.; Cheng, Y.; Chen, L.L.; Luo, Q.; Xu, W.J.; Cao, L.S.; Duan, X.C.; Hu, Z.K. Testing the Universality of Free Fall by Comparing the Atoms in Different Hyperfine States with Bragg Diffraction. *Chin. Phys. Lett.* **2020**, *37*, 043701. [CrossRef]

125. Xu, Y.Y.; Deng, X.B.; Duan, X.C.; Cao, L.S.; Zhou, M.K.; Shao, C.G.; Hu, Z.K. de-Broglie wavelength enhanced weak equivalence principle test for atoms in different hyperfine states. *arXiv* **2022**, arXiv:2210.08533.

126. Damour, T. Testing the equivalence principle: Why and how? *Class. Quantum Gravity* **1996**, *13*, A33. [CrossRef]

127. Hartwig, J.; Abend, S.; Schubert, C.; Schlippert, D.; Ahlers, H.; Posso-Trujillo, K.; Gaaloul, N.; Ertmer, W.; Rasel, E.M. Testing the universality of free fall with rubidium and ytterbium in a very large baseline atom interferometer. *New J. Phys.* **2015**, *17*, 035011. [CrossRef]

128. Tinsley, J.N.; Bandarupally, S.; Chiarotti, M.; Manzoor, S.; Salvi, L.; Poli, N. Prospects for a simultaneous atom interferometer with ultracold cadmium and strontium for fundamental physics tests. In *Proceedings of the Optical and Quantum Sensing and Precision Metrology II*; Scheuer, J., Shahriar, S.M., Eds.; International Society for Optics and Photonics; SPIE: Bellingham, WA, USA, 2022; Volume 12016, p. 1201602. [CrossRef]

129. Altschul, B.; Bailey, Q.G.; Blanchet, L.; Bongs, K.; Bouyer, P.; Cacciapuoti, L.; Capozziello, S.; Gaaloul, N.; Giulini, D.; Hartwig, J.; et al. Quantum tests of the Einstein Equivalence Principle with the STE–QUEST space mission. *Adv. Space Res.* **2015**, *55*, 501–524. [CrossRef]

130. Williams, J.; wey Chiow, S.; Yu, N.; Müller, H. Quantum test of the equivalence principle and space-time aboard the International Space Station. *New J. Phys.* **2016**, *18*, 025018. [CrossRef]

131. Cacciapuoti, L.; de Angelis, M.; Fattori, M.; Lamporesi, G.; Petelski, T.; Prevedelli, M.; Stuhler, J.; Tino, G.M. Analog+digital phase and frequency detector for phase locking of diode lasers. *Rev. Sci. Instrum.* **2005**, *76*, 053111. [CrossRef]

132. Tackmann, G.; Gilowski, M.; Schubert, C.; Berg, P.; Wendrich, T.; Ertmer, W.; Rasel, E.M. Phase-locking of two self-seeded tapered amplifier lasers. *Opt. Express* **2010**, *18*, 9258–9265. [CrossRef] [PubMed]

133. Lenef, A.; Hammond, T.D.; Smith, E.T.; Chapman, M.S.; Rubenstein, R.A.; Pritchard, D.E. Rotation Sensing with an Atom Interferometer. *Phys. Rev. Lett.* **1997**, *78*, 760–763. [CrossRef]

134. Müller, H.; Chiow, S.W.; Long, Q.; Herrmann, S.; Chu, S. Atom Interferometry with up to 24-Photon-Momentum-Transfer Beam Splitters. *Phys. Rev. Lett.* **2008**, *100*, 180405. [CrossRef]

135. Weitz, M.; Young, B.C.; Chu, S. Atomic Interferometer Based on Adiabatic Population Transfer. *Phys. Rev. Lett.* **1994**, *73*, 2563–2566. [CrossRef]

136. Shahriar, M.; Turukhin, A.; Liptay, T.; Tan, Y.; Hemmer, P. Demonstration of injection locking a diode laser using a filtered electro-optic modulator sideband. *Opt. Commun.* **2000**, *184*, 457–462. [CrossRef]

137. Yim, S.H.; Lee, S.B.; Kwon, T.Y.; Park, S.E. Optical phase locking of two extended-cavity diode lasers with ultra-low phase noise for atom interferometry. *Appl. Phys. B* **2014**, *115*, 491–495. [CrossRef]

138. Wang, K.; Yao, Z.; Li, R.; Lu, S.; Chen, X.; Wang, J.; Zhan, M. Hybrid wide-band, low-phase-noise scheme for Raman lasers in atom interferometry by integrating an acousto-optic modulator and a feedback loop. *Appl. Opt.* **2016**, *55*, 989–992. [CrossRef] [PubMed]

139. Weitz, M.; Young, B.C.; Chu, S. Atom manipulation based on delayed laser pulses in three- and four-level systems: Light shifts and transfer efficiencies. *Phys. Rev. A* **1994**, *50*, 2438–2444. [CrossRef]

140. Li, R.B.; Zhou, L.; Wang, J.; Zhan, M.S. Measurement of the quadratic Zeeman shift of 85Rb hyperfine sublevels using stimulated Raman transitions. *Opt. Commun.* **2009**, *282*, 1340–1344. [CrossRef]

141. Zhu, L.; Lien, Y.H.; Hinton, A.; Niggebaum, A.; Rammeloo, C.; Bongs, K.; Holynski, M. Application of optical single-sideband laser in Raman atom interferometry. *Opt. Express* **2018**, *26*, 6542–6553. [CrossRef]

142. Rammeloo, C.; Zhu, L.; Lien, Y.H.; Bongs, K.; Holynski, M. Performance of an optical single-sideband laser system for atom interferometry. *J. Opt. Soc. Am. B* **2020**, *37*, 1485–1493. [CrossRef]

143. Luo, Q.; Zhang, H.; Zhang, K.; Duan, X.C.; Hu, Z.K.; Chen, L.L.; Zhou, M.K. A compact laser system for a portable atom interferometry gravimeter. *Rev. Sci. Instrum.* **2019**, *90*, 043104. [CrossRef]

144. McGuirk, J.M.; Snadden, M.J.; Kasevich, M.A. Large Area Light-Pulse Atom Interferometry. *Phys. Rev. Lett.* **2000**, *85*, 4498–4501. [CrossRef]

145. Hu, L.; Poli, N.; Salvi, L.; Tino, G.M. Atom Interferometry with the Sr Optical Clock Transition. *Phys. Rev. Lett.* **2017**, *119*, 263601. [CrossRef]

146. Hamilton, P.; Jaffe, M.; Brown, J.M.; Maisenbacher, L.; Estey, B.; Müller, H. Atom Interferometry in an Optical Cavity. *Phys. Rev. Lett.* **2015**, *114*, 100405. [CrossRef] [PubMed]

147. Nourshargh, R.; Lellouch, S.; Hedges, S.; Langlois, M.; Bongs, K.; Holynski, M. Circulating pulse cavity enhancement as a method for extreme momentum transfer atom interferometry. *Commun. Phys.* **2021**, *4*, 257. [CrossRef]

148. Yao, Z.W.; Lu, S.B.; Li, R.B.; Luo, J.; Wang, J.; Zhan, M.S. Calibration of atomic trajectories in a large-area dual-atom-interferometer gyroscope. *Phys. Rev. A* **2018**, *97*, 013620. [CrossRef]

149. Zhu, L.; Zhong, J.; Zhang, X.; Lyu, W.; Liu, W.; Xu, W.; Chen, X.; Wang, J.; Zhan, M. Feedback control of atom trajectories in a horizontal atom gravity gradiometer. *Opt. Express* **2022**, *30*, 10071–10083. [CrossRef]

150. Rocco, E.; Palmer, R.N.; Valenzuela, T.; Boyer, V.; Freise, A.; Bongs, K. Fluorescence detection at the atom shot noise limit for atom interferometry. *New J. Phys.* **2014**, *16*, 093046. [CrossRef]

151. Biedermann, G.W.; Wu, X.; Deslauriers, L.; Takase, K.; Kasevich, M.A. Low-noise simultaneous fluorescence detection of two atomic states. *Opt. Lett.* **2009**, *34*, 347–349. [CrossRef]

152. Song, H.; Zhong, J.; Chen, X.; Zhu, L.; Wang, Y.; Wang, J.; Zhan, M. Normalized detection by using the blow-away signal in cold atom interferometry. *Opt. Express* **2016**, *24*, 28392–28399. [CrossRef]

153. Foster, G.T.; Fixler, J.B.; McGuirk, J.M.; Kasevich, M.A. Method of phase extraction between coupled atom interferometers using ellipse-specific fitting. *Opt. Lett.* **2002**, *27*, 951–953. [CrossRef]

154. Stockton, J.K.; Wu, X.; Kasevich, M.A. Bayesian estimation of differential interferometer phase. *Phys. Rev. A* **2007**, *76*, 033613. [CrossRef]

155. Varoquaux, G.; Nyman, R.A.; Geiger, R.; Cheinet, P.; Landragin, A.; Bouyer, P. How to estimate the differential acceleration in a two-species atom interferometer to test the equivalence principle. *New J. Phys.* **2009**, *11*, 113010. [CrossRef]

156. Chen, X.; Zhong, J.; Song, H.; Zhu, L.; Wang, J.; Zhan, M. Proportional-scanning-phase method to suppress the vibrational noise in nonisotope dual-atom-interferometer-based weak-equivalence-principle-test experiments. *Phys. Rev. A* **2014**, *90*, 023609. [CrossRef]

157. Wang, Y.P.; Zhong, J.Q.; Chen, X.; Li, R.B.; Li, D.W.; Zhu, L.; Song, H.W.; Wang, J.; Zhan, M.S. Extracting the differential phase in dual atom interferometers by modulating magnetic fields. *Opt. Commun.* **2016**, *375*, 34–37. [CrossRef]

158. Hu, J.G.; Chen, X.; Wang, L.Y.; Liao, Q.H.; Wang, Q.N. Systematic error suppression scheme of the weak equivalence principle test by dual atom interferometers in space based on spectral correlation. *Chin. Phys. B* **2020**, *29*, 110305. [CrossRef]

159. Antoine, C.; Bordé, C.J. Quantum theory of atomic clocks and gravito-inertial sensors: An update. *J. Opt. B Quantum Semiclass. Opt.* **2003**, *5*, S199. [CrossRef]

160. Roura, A. Circumventing Heisenberg's Uncertainty Principle in Atom Interferometry Tests of the Equivalence Principle. *Phys. Rev. Lett.* **2017**, *118*, 160401. [CrossRef]

161. D'Amico, G.; Rosi, G.; Zhan, S.; Cacciapuoti, L.; Fattori, M.; Tino, G.M. Canceling the Gravity Gradient Phase Shift in Atom Interferometry. *Phys. Rev. Lett.* **2017**, *119*, 253201. [CrossRef]

162. Chiow, S.; Williams, J.; Yu, N.; Müller, H. Gravity-gradient suppression in spaceborne atomic tests of the equivalence principle. *Phys. Rev. A* **2017**, *95*, 021603. [CrossRef]

163. Duan, W.T.; He, C.; Yan, S.T.; Ji, Y.H.; Zhou, L.; Chen, X.; Wang, J.; Zhan, M.S. Suppression of Coriolis error in weak equivalence principle test using 85Rb–87Rb dual-species atom interferometer. *Chin. Phys. B* **2020**, *29*, 070305. [CrossRef]

164. Lan, S.Y.; Kuan, P.C.; Estey, B.; Haslinger, P.; Müller, H. Influence of the Coriolis Force in Atom Interferometry. *Phys. Rev. Lett.* **2012**, *108*, 090402. [CrossRef]

165. Louchet-Chauvet, A.; Farah, T.; Bodart, Q.; Clairon, A.; Landragin, A.; Merlet, S.; Santos, F.P.D. The influence of transverse motion within an atomic gravimeter. *New J. Phys.* **2011**, *13*, 065025. [CrossRef]

166. Schkolnik, V.; Leykauf, B.; Hauth, M.; Freier, C.; Peters, A. The effect of wavefront aberrations in atom interferometry. *Appl. Phys. B* **2015**, *120*, 311–316. [CrossRef]

167. Hu, J.; Chen, X.; Fang, J.; Zhou, L.; Zhong, J.; Wang, J.; Zhan, M. Analysis and suppression of wave-front-aberration phase noise in weak-equivalence-principle tests using dual-species atom interferometers. *Phys. Rev. A* **2017**, *96*, 023618. [CrossRef]

168. Wang, Z.; Chen, T.; Wang, X.; Zhang, Z.; Xu, Y.; Lin, Q. A precision analysis and determination of the technical requirements of an atom interferometer for gravity measurement. *Front. Phys. China* **2009**, *4*, 174–178. [CrossRef]

169. Zhou, M.; Luo, Q.; Chen, L.; Duan, X.; Hu, Z. Observing the effect of wave-front aberrations in an atom interferometer by modulating the diameter of Raman beams. *Phys. Rev. A* **2016**, *93*, 043610. [CrossRef]

170. Trimeche, A.; Langlois, M.; Merlet, S.; Pereira Dos Santos, F. Active Control of Laser Wavefronts in Atom Interferometers. *Phys. Rev. Appl.* **2017**, *7*, 034016. [CrossRef]

171. Karcher, R.; Imanaliev, A.; Merlet, S.; Santos, F.P.D. Improving the accuracy of atom interferometers with ultracold sources. *New J. Phys.* **2018**, *20*, 113041. [CrossRef]

172. Chamakhi, R.; Ahlers, H.; Telmini, M.; Schubert, C.; Rasel, E.M.; Gaaloul, N. Species-selective lattice launch for precision atom interferometry. *New J. Phys.* **2015**, *17*, 123002. [CrossRef]

173. Hu, Q.Q.; Freier, C.; Leykauf, B.; Schkolnik, V.; Yang, J.; Krutzik, M.; Peters, A. Mapping the absolute magnetic field and evaluating the quadratic Zeeman-effect-induced systematic error in an atom interferometer gravimeter. *Phys. Rev. A* **2017**, *96*, 033414. [CrossRef]

174. Wodey, E.; Tell, D.; Rasel, E.M.; Schlippert, D.; Baur, R.; Kissling, U.; Kölliker, B.; Lorenz, M.; Marrer, M.; Schläpfer, U.; et al. A scalable high-performance magnetic shield for very long baseline atom interferometry. *Rev. Sci. Instrum.* **2020**, *91*, 035117. [CrossRef]

175. Ji, Y.H.; Zhou, L.; Yan, S.T.; He, C.; Zhou, C.; Barthwal, S.; Yang, F.; Duan, W.T.; Zhang, W.D.; Xu, R.D.; et al. An actively compensated 8 nT-level magnetic shielding system for 10-m atom interferometer. *Rev. Sci. Instrum.* **2021**, *92*, 083201. [CrossRef]

176. Hobson, P.; Vovrosh, J.; Stray, B.; Packer, M.; Winch, J.; Holmes, N.; Hayati, F.; McGovern, K.; Bowtell, R.; Brookes, M.; et al. Bespoke magnetic field design for a magnetically shielded cold atom interferometer. *Sci. Rep.* **2022**, *12*, 10520. [CrossRef] [PubMed]

177. Jannin, R.; Cladé, P.; Guellati-Khélifa, S. Phase shift due to atom-atom interactions in a light-pulse atom interferometer. *Phys. Rev. A* **2015**, *92*, 013616. [CrossRef]

178. Horikoshi, M.; Nakagawa, K. Dephasing due to atom-atom interaction in a waveguide interferometer using a Bose-Einstein condensate. *Phys. Rev. A* **2006**, *74*, 031602. [CrossRef]

179. Yao, Z.; Solaro, C.; Carrez, C.; Cladé, P.; Guellati-Khelifa, S. Local phase shift due to interactions in an atom interferometer. *Phys. Rev. A* **2022**, *106*, 043312. [CrossRef]

180. Burchianti, A.; D'Errico, C.; Marconi, L.; Minardi, F.; Fort, C.; Modugno, M. Effect of interactions in the interference pattern of Bose-Einstein condensates. *Phys. Rev. A* **2020**, *102*, 043314. [CrossRef]

181. Zhang, H.; Mao, D.K.; Luo, Q.; Hu, Z.K.; Chen, L.L.; Zhou, M.K. The self-attraction effect in an atom gravity gradiometer. *Metrologia* **2020**, *57*, 045011. [CrossRef]

182. D'Agostino, G.; Merlet, S.; Landragin, A.; Santos, F.P.D. Perturbations of the local gravity field due to mass distribution on precise measuring instruments: A numerical method applied to a cold atom gravimeter. *Metrologia* **2011**, *48*, 299. [CrossRef]

183. Hensley, J.M.; Peters, A.; Chu, S. Active low frequency vertical vibration isolation. *Rev. Sci. Instrum.* **1999**, *70*, 2735–2741. [CrossRef]

184. Tang, B.; Zhou, L.; Xiong, Z.; Wang, J.; Zhan, M. A programmable broadband low frequency active vibration isolation system for atom interferometry. *Rev. Sci. Instrum.* **2014**, *85*, 093109. [CrossRef]

185. Zhou, M.K.; Xiong, X.; Chen, L.L.; Cui, J.F.; Duan, X.C.; Hu, Z.K. Note: A three-dimension active vibration isolator for precision atom gravimeters. *Rev. Sci. Instrum.* **2015**, *86*, 046108. [CrossRef]

186. Bonnin, A.; Zahzam, N.; Bidel, Y.; Bresson, A. Characterization of a simultaneous dual-species atom interferometer for a quantum test of the weak equivalence principle. *Phys. Rev. A* **2015**, *92*, 023626. [CrossRef]

187. Lévèque, T.; Gauguet, A.; Michaud, F.; Pereira Dos Santos, F.; Landragin, A. Enhancing the Area of a Raman Atom Interferometer Using a Versatile Double-Diffraction Technique. *Phys. Rev. Lett.* **2009**, *103*, 080405. [CrossRef] [PubMed]

188. Malossi, N.; Bodart, Q.; Merlet, S.; Lévèque, T.; Landragin, A.; Santos, F.P.D. Double diffraction in an atomic gravimeter. *Phys. Rev. A* **2010**, *81*, 013617. [CrossRef]

189. Deng, X.B.; Duan, X.C.; Mao, D.K.; Zhou, M.K.; Shao, C.G.; Hu, Z.K. Common-mode noise rejection using fringe-locking method in WEP test by simultaneous dual-species atom interferometers. *Chin. Phys. B* **2017**, *26*, 043702. [CrossRef]

190. Abend, S.; Allard, B.; Arnold, A.S.; Ban, T.; Barry, L.; Battelier, B.; Bawamia, A.; Beaufils, Q.; Bernon, S.; Bertoldi, A.; et al. Technology roadmap for cold-atoms based quantum inertial sensor in space. *AVS Quantum Sci.* **2023**, *5*, 019201. [CrossRef]

191. Schuldt, T.; Schubert, C.; Krutzik, M.; Bote, L.G.; Gaaloul, N.; Hartwig, J.; Ahlers, H.; Herr, W.; Posso-Trujillo, K.; Rudolph, J.; et al. Design of a dual species atom interferometer for space. *Exp. Astron.* **2015**, *39*, 167–206. [CrossRef]

192. Hinton, A.; Perea-Ortiz, M.; Winch, J.; Briggs, J.; Freer, S.; Moustoukas, D.; Powell-Gill, S.; Squire, C.; Lamb, A.; Rammeloo, C.; et al. A portable magneto-optical trap with prospects for atom interferometry in civil engineering. *Philos. Trans. R. Soc. A Math. Phys. Eng. Sci.* **2017**, *375*, 20160238. [CrossRef]

193. Lee, J.; Ding, R.; Christensen, J.; Rosenthal, R.R.; Ison, A.; Gillund, D.P.; Bossert, D.; Fuerschbach, K.H.; Kindel, W.; Finnegan, P.S.; et al. A compact cold-atom interferometer with a high data-rate grating magneto-optical trap and a photonic-integrated-circuit-compatible laser system. *Nat. Commun.* **2022**, *13*, 5131. [CrossRef]

194. Fang, J.; Hu, J.; Chen, X.; Zhu, H.; Zhou, L.; Zhong, J.; Wang, J.; Zhan, M. Realization of a compact one-seed laser system for atom interferometer-based gravimeters. *Opt. Express* **2018**, *26*, 1586–1596. [CrossRef]

195. Mazon, M.J.; Iyanu, G.H.; Wang, H. A Portable, Compact Cold Atom Physics Package for Atom Interferometry. In Proceedings of the 2019 Joint Conference of the IEEE International Frequency Control Symposium and European Frequency and Time Forum (EFTF/IFC), Orlando, FL, USA, 14–18 April 2019; pp. 1–5. [CrossRef]

196. Kovachy, T.; Asenbaum, P.; Overstreet, C.; Donnelly, C.A.; Dickerson, S.M.; Sugarbaker, A.; Hogan, J.M.; Kasevich, M.A. Quantum superposition at the half-metre scale. *Nature* **2015**, *528*, 530–533. [CrossRef]

197. He, C.; Yan, S.; Zhou, L.; Barthwal, S.; Xu, R.; Zhou, C.; Ji, Y.; Wang, Q.; Hou, Z.; Wang, J.; et al. All acousto-optic modulator laser system for a 12 m fountain-type dual-species atom interferometer. *Appl. Opt.* **2021**, *60*, 5258–5265. [CrossRef] [PubMed]

198. Zhan, M.S.; Wang, J.; Ni, W.T.; Gao, D.F.; Wang, G.; He, L.X.; Li, R.B.; Zhou, L.; Chen, X.; Zhong, J.Q.; et al. ZAIGA: Zhaoshan long-baseline atom interferometer gravitation antenna. *Int. J. Mod. Phys. D* **2020**, *29*, 1940005. [CrossRef]

199. Müntinga, H.; Ahlers, H.; Krutzik, M.; Wenzlawski, A.; Arnold, S.; Becker, D.; Bongs, K.; Dittus, H.; Duncker, H.; Gaaloul, N.; et al. Interferometry with Bose-Einstein Condensates in Microgravity. *Phys. Rev. Lett.* **2013**, *110*, 093602. [CrossRef] [PubMed]

200. Battelier, B.; Berge, J.; Bertoldi, A.; Blanchet, L.; Bongs, K.; Bouyer, P.; Braxmaier, C.; Calonico, D.; Fayet, P.; Gaaloul, N.; et al. Exploring the foundations of the physical universe with space tests of the equivalence principle. *Exp. Astron.* **2021**, *51*, 1695–1736. [CrossRef]

201. Koenemann, T.; Brinkmann, W.; Goeklue, E.; Laemmerzahl, C.; Dittus, H.; Van Zoest, T.; Rasel, E.M.; Ertmer, W.; Lewoczko-Adamczyk, W.; Schiemangk, M.; et al. A freely falling magneto-optical trap drop tower experiment. *Appl. Phys. B* **2007**, *89*, 431–438. [CrossRef]

202. Stern, G.; Battelier, B.; Geiger, R.; Varoquaux, G.; Villing, A.; Moron, F.; Carraz, O.; Zahzam, N.; Bidel, Y.; Chaibi, W.; et al. Light-pulse atom interferometry in microgravity. *Eur. Phys. J. D* **2009**, *53*, 353–357. [CrossRef]

203. Elsen, M.; Piest, B.; Adam, F.; Anton, O.; Arciszewski, P.; Bartosch, W.; Becker, D.; Böhm, J.; Boles, S.; Döringshoff, K.; et al. A dual-species atom interferometer payload for operation on sounding rockets. *arXiv* **2023**, arXiv:2305.08634.

204. Aguilera, D.N.; Ahlers, H.; Battelier, B.; Bawamia, A.; Bertoldi, A.; Bondarescu, R.; Bongs, K.; Bouyer, P.; Braxmaier, C.; Cacciapuoti, L.; et al. STE-QUEST—test of the universality of free fall using cold atom interferometry. *Class. Quantum Gravity* **2014**, *31*, 115010. [CrossRef]

205. Tino, G.M.; Bassi, A.; Bianco, G.; Bongs, K.; Bouyer, P.; Cacciapuoti, L.; Capozziello, S.; Chen, X.; Chiofalo, M.L.; Derevianko, A.; et al. SAGE: A proposal for a space atomic gravity explorer. *Eur. Phys. J. D* **2019**, *73*, 228. [CrossRef]

206. van Zoest, T.; Gaaloul, N.; Singh, Y.; Ahlers, H.; Herr, W.; Seidel, S.T.; Ertmer, W.; Rasel, E.; Eckart, M.; Kajari, E.; et al. Bose-Einstein Condensation in Microgravity. *Science* **2010**, *328*, 1540–1543. [CrossRef]

207. Aveline, D.C.; Williams, J.R.; Elliott, E.R.; Dutenhoffer, C.; Kellogg, J.R.; Kohel, J.M.; Lay, N.E.; Oudrhiri, K.; Shotwell, R.F.; Yu, N.; et al. Observation of Bose-Einstein condensates in an Earth-orbiting research lab. *Nature* **2020**, *582*, 193–197. [CrossRef] [PubMed]

208. He, M.; Chen, X.; Fang, J.; Chen, Q.; Sun, H.; Wang, Y.; Zhong, J.; Zhou, L.; He, C.; Li, J.; et al. The space cold atom interferometer for testing the equivalence principle in the China Space Station. *NPJ Microgravity* **2023**, *9*, 58. [CrossRef] [PubMed]

209. Belenchia, A.; Carlesso, M.; Bayraktar, Ö.; Dequal, D.; Derkach, I.; Gasbarri, G.; Herr, W.; Li, Y.L.; Rademacher, M.; Sidhu, J.; et al. Quantum physics in space. *Phys. Rep.* **2022**, *951*, 1–70. [CrossRef]

210. Chiow, S.W.; Kovachy, T.; Chien, H.C.; Kasevich, M.A. 102$\hbar k$ Large Area Atom Interferometers. *Phys. Rev. Lett.* **2011**, *107*, 130403. [CrossRef]

211. Plotkin-Swing, B.; Gochnauer, D.; McAlpine, K.E.; Cooper, E.S.; Jamison, A.O.; Gupta, S. Three-Path Atom Interferometry with Large Momentum Separation. *Phys. Rev. Lett.* **2018**, *121*, 133201. [CrossRef]

212. Hensel, T.; Loriani, S.; Schubert, C.; Fitzek, F.; Abend, S.; Ahlers, H.; Siemss, J.N.; Hammerer, K.; Rasel, E.M.; Gaaloul, N. Inertial sensing with quantum gases: A comparative performance study of condensed versus thermal sources for atom interferometry. *Eur. Phys. J. D* **2021**, *75*, 108. [CrossRef]

213. Pezzè, L.; Smerzi, A.; Oberthaler, M.K.; Schmied, R.; Treutlein, P. Quantum metrology with nonclassical states of atomic ensembles. *Rev. Mod. Phys.* **2018**, *90*, 035005. [CrossRef]

214. Anders, F.; Idel, A.; Feldmann, P.; Bondarenko, D.; Loriani, S.; Lange, K.; Peise, J.; Gersemann, M.; Meyer-Hoppe, B.; Abend, S.; et al. Momentum Entanglement for Atom Interferometry. *Phys. Rev. Lett.* **2021**, *127*, 140402. [CrossRef]

215. Overstreet, C.; Asenbaum, P.; Curti, J.; Kim, M.; Kasevich, M.A. Observation of a gravitational Aharonov-Bohm effect. *Science* **2022**, *375*, 226–229. [CrossRef]

216. Nobili, A.M. Fundamental limitations to high-precision tests of the universality of free fall by dropping atoms. *Phys. Rev. A* **2016**, *93*, 023617. [CrossRef]

217. Hohensee, M.A.; Müller, H.; Wiringa, R.B. Equivalence Principle and Bound Kinetic Energy. *Phys. Rev. Lett.* **2013**, *111*, 151102. [CrossRef] [PubMed]

218. Shaniv, R.; Ozeri, R.; Safronova, M.S.; Porsev, S.G.; Dzuba, V.A.; Flambaum, V.V.; Häffner, H. New Methods for Testing Lorentz Invariance with Atomic Systems. *Phys. Rev. Lett.* **2018**, *120*, 103202. [CrossRef] [PubMed]

219. Fortier, T.M.; Ashby, N.; Bergquist, J.C.; Delaney, M.J.; Diddams, S.A.; Heavner, T.P.; Hollberg, L.; Itano, W.M.; Jefferts, S.R.; Kim, K.; et al. Precision Atomic Spectroscopy for Improved Limits on Variation of the Fine Structure Constant and Local Position Invariance. *Phys. Rev. Lett.* **2007**, *98*, 070801. [CrossRef] [PubMed]

220. Bauch, A.; Weyers, S. New experimental limit on the validity of local position invariance. *Phys. Rev. D* **2002**, *65*, 081101. [CrossRef]

221. Zhou, Z. Quantum Test of the Local Position Invariance with Internal Clock Interferometry. *arXiv* **2023**, arXiv:2301.11258.

222. Guéna, J.; Abgrall, M.; Rovera, D.; Rosenbusch, P.; Tobar, M.E.; Laurent, P.; Clairon, A.; Bize, S. Improved Tests of Local Position Invariance Using ^{87}Rb and ^{133}Cs Fountains. *Phys. Rev. Lett.* **2012**, *109*, 080801. [CrossRef]

223. Lange, R.; Huntemann, N.; Rahm, J.M.; Sanner, C.; Shao, H.; Lipphardt, B.; Tamm, C.; Weyers, S.; Peik, E. Improved Limits for Violations of Local Position Invariance from Atomic Clock Comparisons. *Phys. Rev. Lett.* **2021**, *126*, 011102. [CrossRef]

224. Zhang, T.; Chen, L.L.; Shu, Y.B.; Xu, W.J.; Cheng, Y.; Luo, Q.; Hu, Z.K.; Zhou, M.K. Ultrahigh-Sensitivity Bragg Atom Gravimeter and its Application in Testing Lorentz Violation. *Phys. Rev. Appl.* **2023**, *20*, 014067. [CrossRef]